Human Cytomegalovirus Drives WDR5 to the Virion Assembly Compartment to Facilitate Virion Assembly

Bo Yang[1,2], YongXuan Yao[1,2], Hui Wu[3], Hong Yang[4,5], Xue-Hui Ma[4,5], Dong Li[4,5], Xian-Zhang Wang[4,5], Sheng-Nan Huang[4,5], Xuan Jiang[1,2], Shuang Cheng[4], Jin-Yan Sun[4], Zhen-Li Huang[6], CongJian Zhao[7], Michael A. McVoy[8], Jin-Hyun Ahn[9], Wen-Bo Zeng[4], Sitang Gong[1,*,&], William J. Britt[3,*,&], Min-Hua Luo[1,2,4,5,*,&]

[1]Joint Center of Translational Precision Medicine, Guangzhou Institute of Pediatrics, Guangzhou Women and Children Medical Center, Guangzhou, China.

[2]Joint Center of Translational Precision Medicine, Wuhan Institute of Virology, Chinese Academy of Sciences, Wuhan, China.

[3]Department of Pediatrics, University of Alabama School of Medicine, Birmingham, Alabama, USA.

[4]State Key Laboratory of Virology, CAS Center for Excellence in Brain Science and Intelligence Technology, Center for Biosafety Mega-Science, Wuhan Institute of Virology, Chinese Academy of Sciences, Wuhan, China.

[5]University of Chinese Academy of Sciences, Beijing, China.

[6]Britton Chance Center for Biomedical Photonics, Wuhan National Laboratory for Optoelectronics, Huazhong University of Science and Technology, Wuhan, China.

[7]Aier School of Ophthalmology, Aier Eye Institute, Central South University, Changsha, China

[8]Department of Pediatrics, Virginia Commonwealth University School of Medicine, Richmond, Virginia, USA

[9]Department of Molecular Cell Biology, Sungkyunkwan University School of Medicine, Samsung Medical Center, Suwon, Republic of Korea.

Running title: WDR5 Facilitates HCMV Virion Assembly

Keywords: human cytomegalovirus; WDR5; virion structure; virion morphogenesis; virion assembly compartment; vAC.

[*]**Corresponding author:**

luomh@wh.iov.cn (M.L.); sitangg@126.com

wbritt@peds.uab.edu.

[&]M.L., W.B. and S.G. contributed equally to this work.

Abstract (156 words)

We previously reported that human cytomegalovirus (HCMV) utilizes the cellular protein WDR5 to facilitate capsid nuclear egress. Here, we further show that HCMV infection drives WDR5 to the perinuclear region by a mechanism that requires viral replication and intact microtubules. WDR5 accumulated in the virion assembly compartment (vAC) and co-localized with vAC markers of gamma-tubulin (γ-tubulin), early endosomes, and viral vAC marker proteins pp65, pp28, and glycoprotein B (gB). WDR5 interacted with multiple virion proteins, including MCP, pp150, pp65, pIRS1, and pTRS1, which may explain the increasing WDR5 accumulation in the vAC during infection. WDR5 was then incorporated into HCMV virions and localized to the tegument layer, as demonstrated by fractionation and immune-gold electron microscopy. Thus, WDR5 is driven to the vAC and incorporated into virions, suggesting that WDR5 facilitates HCMV replication at later stage of virion assembly besides the capsid nuclear egress stage. These data highlight that WDR5 is a potential target for antiviral therapy.

48 **Importance (127 words)**

49 Human cytomegalovirus (HCMV) has a large (~235-kb) genome that contains
50 over 170 ORFs and exploits numerous cellular factors to facilitate its replication. In
51 the late phase of HCMV infection cytoplasmic membranes are profoundly
52 reconfigured to establish the virion assembly compartment (vAC), which is important
53 for efficient assembly of progeny virions. We previously reported that WDR5
54 promotes HCMV nuclear egress. Here, we show that WDR5 is further driven to the
55 vAC and incorporated into virions, perhaps to facilitate efficient virion maturation.
56 This work identified potential roles for WDR5 in HCMV replication in the
57 cytoplasmic stages of virion assembly. Taken together, WDR5 plays a critical role in
58 HCMV capsid nuclear egress and is important for virion assembly, and thus is a
59 potential target for antiviral treatment of HCMV-associated diseases.

Introduction

Human cytomegalovirus (HCMV) is a ubiquitous pathogen that is highly adapted to its human host. Approximately 50 to 90% of adults are infected globally (1) and in China seroprevalence is as high as 93.7% (2). About 90% of primary HCMV infections in immunocompetent individuals are either asymptomatic or mildly symptomatic. In addition, HCMV is a leading cause of congenital infections worldwide. Following primary infection, the virus remains latent and establishes life-long persistence in its host. However, HCMV can be reactivated and cause severe disease in immunosuppressed or immunodeficient individuals, such as recipients of solid organ or bone marrow transplants and AIDS patients (3-7). In these patients, HCMV infection contributes to multiple end-organ diseases, including pneumonia, gastrointestinal diseases, retinitis, central nervous system diseases, poor engraftment, severe graft-versus-host reaction, and can result in high mortality rates (8-11). In patients receiving hematopoietic stem cell transplantation, the incidence of HCMV disease is as high as 30-70% (12). In addition, congenital HCMV infection is a leading cause of birth defects and is associated with neonatal mortality and permanent developmental sequelae (13-16).

A characteristic feature of HCMV infection is profound remodeling of the secretory and endocytic system (Golgi, trans-Golgi network, and early endosomes) to form nested, cylindrical layers in a structure termed the virion assembly compartment (vAC) (4, 17-22), which is unique in HCMV infection when compared to other herpesviruses (23). Although not essential for virion production, vAC formation has been shown to be necessary for efficient HCMV virion assembly and maturation. Multiple viral and cellular proteins are reported to participate in vAC formation. Viral protein pUL136 is important for vAC formation and efficient virion assembly. Virus

mutants lacking UL136 produce less properly enveloped virions along with a larger number of dense bodies compared to wildtype virus (24). Other viral proteins pUL48, pUL94, and pUL103 are also important for vAC development (21). Interestingly, HCMV-encoded miRNAs UL112-1, US5-1, and US5-2 target host secretory pathway factors to facilitate vAC formation (25). Cellular proteins, including RhoB (22), IFITMs (23), STX5 (26), dynein (27), BiP (27, 28), Bicaudal D1 (29), Rab11 and FIP4 (30), have also been shown to localize to vAC.

A number of cellular proteins are relocated to the vAC and subsequently incorporated into virions. Proteomic analyses have identified over 70 viral and cellular proteins in HCMV virions. Virion-associated cellular proteins are involved in a wide range of processes and functions, including ATP binding, Ca^{2+} signaling, signal transduction, transcription, and translation (31). WD repeat-containing protein 5 (WDR5) is a highly conserved WD-40 repeat protein that is critical for regulating multiple cellular processes. The most common function of WD-repeat proteins is to serve as a rigid scaffold for protein-protein interactions, which facilitates formation and/or stabilization of multi-protein complexes (32), such as MOF (males absent on the first)-containing NSL (33), KANSL1 and KANSL2 (33), and histone H3 at lysine 4 (H3K4) methyltransferases of the SET1-family (Set1A, Set1B, MLL1, MLL2, MLL3, and MLL4) (34-37). Thus, previous studies of WDR5 have focused on epigenetics (38-41); however, WDR5 can also stabilize actin architecture to promote multi-ciliated cell formation (42) and is important for embryonic stem cell reprogramming, self-renewal, and maintenance of pluripotency (43, 44).

The role of WDR5 in RNA virus infections has also been investigated. Upon Sendai virus infection, WDR5 is translocated from the nucleus to the mitochondria and is essential for formation of the VISA-associated complex (45). Measles virus

recruits WDR5 into viral inclusion bodies in the cytoplasm to facilitate virus replication (46). Our previous work showed that WDR5 promotes HCMV replication through facilitating capsid nuclear egress (47). In the present study, we further demonstrate that in HCMV-infected cells WDR5 protein levels increase in the cytoplasm and that WDR5 is translocated to and accumulates in the vAC. The accumulated WDR5 is incorporated into and localizes within the tegument layer of virions which facilitates virion morphogenesis.

Results

Perinuclear accumulation of WDR5 is induced by HCMV infection. It has been reported that cellular protein WDR5 is translocated from the nucleus to mitochondria during Sendai virus infection and to viral replication centers during measles virus infection. As both are RNA viruses (45, 46), we sought to investigate whether a corresponding WDR5 relocation occurs during HCMV infection. We initially determined if WDR5 is redistributed during HCMV infection of immortalized human embryonic lung fibroblasts (HELFs). In mock-infected HELFs, WDR5 had diffuse nuclear localization with a single small perinuclear punctum which coincided with MTOC, whereas in HCMV-infected cells WDR5 was clearly localized in a perinuclear region (Fig 1A). To exclude the possibility that WDR5 perinuclear accumulation is limited to HELFs or infection by HCMV strain Towne, similar experiments were performed with primary cell HELs and U251 glioma cells infected with HCMV strains Towne or AD169, and similar perinuclear WDR5 localization was observed (data not shown). In addition, similar perinuclear localization was also observed during murine cytomegalovirus (MCMV) infection of mouse NIH3T3 fibroblasts (Fig 1B). Interestingly, this effect was not observed during infection of HELFs by other DNA viruses that have not been reported to form vAC-like structures during infection, including herpes simplex virus type 1 (HSV-1), varicella-zoster virus (VZV), adenovirus (AdV), or autographa californica multiple nuclear polyhedrosis virus (AcMNPV) (Fig 1C). These data suggest that the perinuclear accumulation of WDR5 is specifically induced by HCMV or MCMV infection.

WDR5 perinuclear accumulation progresses with HCMV infection. To gain further insights into changes in subcellular localization of WDR5 during HCMV

infection, a time course confocal microscopy study was performed from 12 to 96 hpi. Focal perinuclear accumulation of WDR5 was first observed at 24 hpi and increased as the infection progressed (Fig 2A and B).

To further investigate the impact of HCMV infection on WDR5 and its cytosolic/nuclear distribution, HCMV- and mock-infected cells were harvested at 96 hpi and cytosolic and nuclear fractions were analyzed by immunoblot (IB). The efficiency of nuclear and cytosolic fractionation was confirmed by probing for cellular markers GAPDH and Lamin B1, which localize to cytoplasm and nuclei, respectively, as well as for viral proteins pp28 (pUL99) and IE1, which also localize to the cytosol and nucleus, respectively (Fig 2C). In mock-infected cells, WDR5 was located in the nuclear fraction and at a much lower level in the cytosol. In contrast, HCMV-infected cells contained less WDR5 protein in the nuclear fraction, while with a significantly higher level of WDR5 protein in the cytosolic fraction (Fig 2C). Previous studies have shown that nuclear membranes are significantly remodeled during HCMV infection (27). To exclude a possibility that higher cytosolic protein level of WDR5 was a result from simple diffusion, leptomycin B (LMB) was used to inhibit nuclear export. Nuclear retention of WDR5 was clearly observed and perinuclear accumulation of WDR5 was prevented by LMB treatment (Fig 2D). These data suggested that nuclear WDR5 relocated to the cytoplasm during HCMV infection is not due to diffusion.

WDR5 perinuclear accumulation requires viral replication. To determine the kinetic class of viral gene expression required to alter WDR5 localization, HELFs were incubated with HCMV virions that were UV-irradiated to block all *de novo* viral gene expression or with infectious virions in the presence of the viral DNA polymerase inhibitors ganciclovir (GCV) or phosphonoacetic acid (PAA) to block

viral DNA synthesis and late gene expression. Immunoblot at 72 hpi confirmed that UV irradiation blocked expression of all viral proteins tested, including IE1/IE2, the early/late protein pUL44, and the true late glycoprotein B (gB). In contrast, infection in the presence of either GCV or PAA had no effect on IE1, while IE2 and pUL44 levels were reduced, and, as predicted for a late protein, gB expression was fully blocked (Fig 3A). WDR5 protein and mRNA levels were compared during HCMV infection with or without GCV or PAA treatment. Compared to the mock-infected group, both WDR5 protein (Fig 3A) and mRNA levels (Fig. 3B) were elevated in virus-infected cells in both presence and absence of GCV or PAA. In HCMV-infected cells WDR5 protein levels were not significantly altered by GCV or PAA treatment.

We further investigated whether WDR5 perinuclear accumulation is altered by treatment of GCV or PAA. Characterization of replicate cultures by immunofluorescence revealed that WDR5 localization was similar to that in mock infected cells when virions were inactivated by exposure to UV. Both GCV and PAA dramatically inhibited perinuclear accumulation of WDR5 and perinuclear foci formation (Fig 3C). Although the expression of WDR5 was elevated by virus infection in the presence of GCV and PAA (Fig 3A and 3B), the perinuclear-accumulated WDR5 was still dramatically inhibited. These results indicated that WDR5 perinuclear accumulation and perinuclear foci formation are not due to increasing WDR5 levels, but are due to relocalization of WDR5 by a process that requires HCMV DNA synthesis and/or *de novo* synthesis of viral late proteins.

Accumulation of WDR5 in perinuclear vACs requires microtubule polymerization. The location, morphology, and dependence on viral late gene expression suggested that WDR5 may be accumulating in the vAC. To confirm this

192 possibility, colocalization of WDR5 with the vAC markers was examined. At 72 hpi,
193 WDR5 accumulated in a juxtanuclear region in cells with kidney-shaped nuclei that
194 also displayed cytoskeletal filaments (alpha-tubulin) radiating out to the rim of the
195 plasma membrane (Fig 4A, a to d). This region also co-localized with gamma-tubulin
196 (Fig 4A, e to h), which is the marker of the microtubule organizing center (MTOC)
197 (48). This juxtanuclear region was wrapped around by a tightly nested ring of Golgi
198 elements (anti-58K, Fig 4A, i to l) and colocalized well with early endosome marker
199 EEA1 (Fig 4A, m to p). These characteristics have all been reported for the vAC (18),
200 and confirmed that WDR5 accumulates in the vAC.

201 To determine if WDR5 accumulation in the vAC was microtubule dependent
202 similar to virion structural proteins such as pp150 (29), replicate cultures to those
203 shown in Fig 4A were treated with nocodazole (NOC) to disrupt microtubule
204 polymerization (49) and analyzed by IFA after 20 min, 4h, or 6h of NOC treatment.
205 While γ-tubulin was less sensitive to NOC treatment (Fig 4B, c and g), α-tubulin
206 filaments became fragmented and punctate in distribution after 4-6 h NOC treatment
207 (Fig 4B, k and o). Concomitant with the fragmentation of microtubules, WDR5
208 perinuclear foci dispersed (Fig 4B, f, j and n).

209 In HCMV-infected cells, the vAC is enriched in various viral capsid, tegument,
210 and envelope proteins (17, 18). To further confirm that accumulation of WDR5 in
211 perinuclear foci resulted from recruitment of WDR5 to the vAC, infected cells were
212 co-stained for WDR5 and viral vAC markers, including the tegument proteins pp28
213 and pp65 and the envelope glycoprotein gB (18). As shown in Fig 4C, pp28, pp65,
214 and gB closely colocalized with WDR5. A three-dimensional (3-D) reconstruction
215 from Z-stack images of the cell shown in the bottom panel of Fig 4C clearly

demonstrated the colocalization of WDR5 with vAC marker gB. All these data indicated that WDR5 was driven to vAC during HCMV infection.

WDR5 plays a crucial role in vAC formation and virion morphogenesis.

To further explore whether WDR5 contributes to formation of vAC, we used a previously described pair of HELF-derived cell lines, one in which WDR5 is knocked down by shRNA (KD) and one expressing an irrelevant control shRNA (Ctl) (47). In KD cells, WDR5 knockdown altered formation and/or morphology of vAC, as determined by staining for gB. Irregular vAC exhibited multiple juxtanuclear foci, while in some infected cells no distinct vAC was observed (Fig 5A). Since proper vAC formation is necessary for efficient HCMV virion assembly and maturation. We further examine the virion morphogenesis by TEM in Ctl and KD cells. We previously have reported that knockdown of WDR5 dramatically decreased the number of matured virions in the vAC (47). As shown in Fig 5B (f to k), knockdown of WDR5 resulted in decrease of mature virions and distinct defects in virion maturation (white arrow). Nearly 39% of viral particles lacked envelope in KD cells (Fig. 5C). Inhibition of viral replication (Fig 3A and C) and disrupting microtubules (Fig 4B) both affect WDR5 accumulation in vAC, knock down WDR5 by shRNA altered formation and/or morphology of vAC (Fig 4D). All these data strongly support that WDR5 plays a crucial role in vAC formation and virion morphogenesis.

The N-terminal domain of WDR5 is critical for WDR5 accumulation in vAC. The functional implementation of a protein depends on its subcellular distribution. To dissect which domain of WDR5 is critical for its accumulation in the vAC, a serial mutant of WDR5 were constructed based on its structure. WDR5 contains seven

typical WD40 repeat domains (WD1 to WD7, Fig 6A), each WD40 repeat motif forms a blade β-propeller (37). A series of WDR5 deletion mutants were constructed as illustrated in Fig 6A. The distribution of Flag-tagged full-length WDR5 and the indicated mutants were determined. All the WDR5 constructs were transfected into HELF cells for 24 h, followed by either mock- or HCMV-infection at an MOI of 3. The full-length WDR5 showed a predominant nuclear localization in mock-infected HELFs, which is consistent with the results for endogenous WDR5 described above, accumulated in vAC in infected cells. Two mutants, Flag-aa1-82 and Flag-aa1-42, which retained the N-terminal amino acids 1-42, showed pan-cellular distribution upon mock-infection but still localized to vAC upon HCMV infection. In contrast, mutants lacking the amino acids 1-42 displayed mainly nuclear localization (*e.g.*, Flag-aa43-334) or pan-cellular distribution, and were not relocalized to vAC during HCMV infection. Taken together, these data indicate that the N-terminal amino acids 1-42 of WDR5 are critical for WDR5 accumulation in vACs.

WDR5 co-fractionates with HCMV particles. Since WDR5 accumulated in the vAC, we next sought to determine if WDR5 is incorporated into viral particles. HELFs were mock- or HCMV-infected and cells were lysed by sonication. Intra- and extracellular particles were combined and then analyzed by iodixanol density gradient centrifugation, as illustrated in Fig 7A. Fractions were collected from top to bottom of the gradient, and analyzed by immuno-dot-blot for the presence of WDR5, gB, or pUL48, and for viral DNA by qPCR. WDR5 was undetectable in all fractions derived from mock-infected cultures (Fig 7B). In contrast, WDR5 was detected in fractions derived from HCMV-infected cultures and fractions with peak levels of WDR5

265 corresponded with those containing peak levels of gB, pUL48, and viral DNA (Fig 7B
266 and 7C), suggesting that WDR5 is associated with HCMV particles.
267
268 **WDR5 is present in the tegument layer of HCMV virions.** To determine whether
269 WDR5 is incorporated into virions, extracellular virions were purified from infected-
270 cell culture supernatants as described previously (50). The purified virions were then
271 either mock treated or treated with 2% Triton X-100 at room temperature for 1 h,
272 layered onto a 10% to 50% iodixanol continuous gradient, and ultra-centrifuged at
273 100,000 × *g* for 2 h. Fractions were collected from top to bottom of the gradient and
274 analyzed by IB for WDR5, structural viral proteins, including major capsid protein
275 (MCP), tegument proteins pp28, pp65, pp71, pIRS1, pTRS1, pUL48, and the
276 envelope glycoprotein B (gB), as well as the non-structural viral proteins IE1/2 and
277 pUL44. IE1/2 and pUL44 were present in infected-cell lysates but were not in any
278 gradient fractions, confirming effective separation of virions from infected-cells (Fig
279 8A). In gradient fractions of mock-treated virions, fractions 9 and 10 contained peak
280 levels of MCP, tegument proteins, gB, and WDR5 (Fig 8A, upper panel). In gradient
281 fractions of Triton X-100-treated virions, peak levels of MCP and tegument proteins
282 shifted to fraction 11, while the majority of gB and a fraction of the outer tegument
283 protein pp28 shifted to lower density fractions and no longer co-fractionated with
284 MCP (Fig 8A, lower panel). These results suggested that Triton X-100 treatment
285 removed the envelope and some of the outer tegument layers from the virion particles.
286 The finding that WDR5 remained predominantly in fraction 11 following Triton X-
287 100 treatment (Fig 8A, lower panel) suggested that WDR5 was either associated with
288 the inner tegument layers or was directly attached to capsids.

Immunogold labeling was next used to further examine WDR5 association with virions. Purified virions were again either mock treated or treated with Triton X-100 (as described above) to allow access of antibodies to proteins in the inner layers of treated viral particles. The particles were then labeled with mAbs to gB, pp28, or WDR5 followed by immunogold labeling and detection by electron microscopy. Consistent with the established presence of gB in the virion envelope, gold particles were observed decorating the surface of mock-treated particles labeled using anti-gB antibody (Fig 8B, panel a). In contrast, and consistent with the known localization of pp28 in the tegument of the virion, gold particles were observed decorating the surface of Triton X-100-treated particles labeled using anti-pp28 antibody (Fig 8B, panel b). Immunogold labeling with anti-WDR5 antibody was similar to that of pp28, suggesting that WDR5 was localized within the tegument layer (Fig 8B, panel c). Moreover, capsids purified from infected-cell nuclei (before nuclear egress) or from virions purified from culture supernatants both contained WDR5 (Fig. 8C).

Taken together, these results indicate that WDR5 is associated with capsids before nuclear egress, translocates to and accumulates in vAC, finally incorporates into virion tegument layer, which is critical for virion morphogenesis.

WDR5 interacts with viral structural proteins. The above findings indicate that WDR5 is associated with capsids before nuclear egress, then accumulates in the vAC, and is ultimately incorporated into virions. We therefore infer that WDR5 likely interacts with one or more viral structural proteins. To test this hypothesis, Flag-tagged WDR5 was overexpressed in HELF cells followed by mock- or HCMV-infection for 96 h. Cell lysates were immunoprecipitated (IP) with anti-Flag antibody and subjected to SDS-PAGE and Coomassie staining. There were four different

distinct protein species (Fig. 9A, red arrows) in the viral-infected immunoprecipitates when compared to the mock control. These four species were further analyzed by liquid chromatography-tandem mass spectrometry (LC-MS/MS) to identify and quantify the proteins. As shown in Fig 9B, viral structural proteins, including MCP, pp150, pp65, pIRS1, and pTRS1, were identified in the immunoprecitates.

To confirm WDR5-viral protein interactions, HEK293T cells were co-transfected with plasmids expressing HA-tagged WDR5 and each of the candidate viral protein interactors (Myc-MCP, Flag-pp65, Myc-pp150, Flag-pIRS1, or V5-pTRS1). Each viral protein was immunoprecipitated using their respective epitope tags and the immunoprecipitates were then probed for WDR5 by IB for the HA tag. WDR5-HA could be detected in IPs for MCP, pp65, pp150, pIRS1, and pTRS1 but not for pp28 or the IgG controls (Fig. 9C-H). Taken together, these results indicate that WDR5 interacts with viral structural proteins, which explains its accumulation in vAC and its role in facilitating mature virion morphogenesis.

Discussion

During the course of a viral infection, cellular proteins can be incorporated into viral particles. For example, both LC-MS/MS and multidimensional protein identification technology (MudPIT) have been used to identify components of influenza virions, and while seventeen virion-associated cellular proteins were identified by both methods, six others were identified only with the LC-MS/MS analysis and 13 were identified only with MudPIT analysis (51), suggesting that multiple approaches may be necessary to identify all of the virion-associated cellular factors. In some cases, cellular proteins are incorporated randomly and have not been shown to play a role in the infectivity of the mature virion, whereas in other cases cellular proteins are selectively incorporated into virions through specific interactions with virion structural proteins or the viral genome. With regard to HCMV, LC-MS/MS has identified over 70 host proteins in virions. These cellular proteins function in diverse processes, including ATP and Ca^{2+} binding, chaperones, cytoskeleton, enzymatic activities, glycolysis, protein transport, signal transduction, transcription, and translation (31). Some have been reported to function during certain stages of the infection process, suggesting that these proteins are incorporated into the virion to facilitate virus infectivity and replication (31). Others may serve to evade host immune mechanisms; for example, in the late stage of infection intracellular viral DNA sensors and restriction factors such as IFI16 traffic to vAC where they are incorporated into mature virions (52).

Previously, we found that HCMV infection increases WDR5, and WDR5 facilitates capsid nuclear egress (47). In the present study we analyzed the cellular distribution of WDR5 and observed that the distribution of WDR5 was altered by HCMV infection, as it accumulated in vAC. Treatment with viral replication

355 inhibitors (GCV or PAA) and microtubule polymerization inhibitor (NOC)
356 significantly prevented WDR5 accumulation in the vAC. Inhibition of viral
357 replication, including viral DNA replication and expression of late viral structure
358 proteins, impairs formation of the vAC. The vAC formation is also dissolved by
359 microtubule polymerization inhibitor. Under both conditions, the protein levels of
360 WDR5 are not significantly changed, but vAC formation is dramatically impaired.
361 Thus, relocation and accumulation of WDR5 in vAC requires HCMV late gene
362 expression and depends on microtubule polymerization. Taken together, these
363 findings suggest that WDR5 accumulation in the vAC occurs as a result of a specific
364 HCMV-dependent mechanism, although this mechanism remains undefined.

365 In order to determine if WDR5 was incorporated into virions, we analyzed intra-
366 and extracellular viral particles and purified virions for the presence of WDR5 after
367 purification of virion particles by density gradient centrifugation. In each case WDR5
368 cofractionated with markers for virions or capsid particles but was not detected in
369 gradient fractions derived from uninfected cultures. Furthermore, we showed that
370 WDR5 interacts with virion tegument proteins pp65, pIRS1, and pTRS1. Therefore,
371 we propose that WDR5 resides within the tegument layer of HCMV virions. To
372 investigate the location of WDR5 in virions, we treated virions with Triton X-100, a
373 detergent that solubilizes virion membranes. Following Triton X-100 treatment, a
374 significant amount of WDR5 remained associated with the detergent treated virions.
375 In addition, immuno-gold electron microscopy indicated that WDR5 was present
376 within virions and was localized to the tegument. These data, together with our
377 previous findings that WDR5 plays a role in the assembly of the NEC and capsid
378 egress, suggest that during nuclear egress WDR5 may initially enter the perinuclear
379 cisterna together with capsids and travels along with capsids to the cytoplasm and

vAC (Fig 10). WDR5 then interacts with viral structural proteins (*e.g.*, MCP, pp150, and pp65), thereby accumulating in vAC; finally, WDR5 is packaged into virions along with numerous tegument proteins and glycoproteins.

In summary, the data provided in this study suggest a dual role for WDR5 during HCMV assembly. During nuclear egress, it modulates NEC assembly and facilitates capsid nuclear egress. Subsequently, it translocates along with capsid from the nucleus into the cytoplasm by interacting with MCP; it accumulates in vAC by interacting with multiple late viral structures proteins and is incorporated into virions. Since WDR5 interacts with multiple viral structure proteins, it could function during virion morphogenesis by stabilizing multi-protein complexes. WDR5 plays a critical role in capsid nuclear egress, vAC formation, and virion assembly. Our findings further demonstrate that HCMV manipulates existing cellular mechanisms, including the localization of cellular proteins, to facilitate its replication, assembly, and egress. These data highlight that WDR5 is a potential new target for antiviral drug development.

Acknowledgements

We thank Dr. Hua Zhu from Rutgers-New Jersey Medical School for providing VZV Oka strain, Qiyi Tang from Howard University College of Medicine for providing MCMV K181 strain, and Drs. Zhengli Shi and Zhihong Hu from Wuhan Institute of Virology, CAS, for providing GFP-expressing AdV and AcMNPV, respectively. We thank Dr. Wade Gibson from Johns Hopkins University for providing pUL48 rabbit serum, Dr. Yan Zhou from Wuhan University for providing γ-Tubulin antibody, and Dr. Thomas E. Shenk from Princeton University for providing pIRS1 and pTRS1 antibodies. We thank Dr. Adam P. Geballe from Fred Hutchinson Cancer Research Center, University of Washington for providing pTRS1 expressing plasmid. We thank Ding Gao, Anna Du, and Pei Zhang of The Core Facility, Wuhan Institute of Virology, CAS, for technical support of electron microscopy.

Conflict of interest

The authors declared that they have no conflicts of interest to this work.

Funding

This work was supported by grants from the National Natural Science Foundation of China (81620108021, 81427801, 31900137 and 31900138), and China Postdoctoral Science Foundation (2019M652846 and 2019M662851).

Materials and Methods

Ethics statement. Human embryonic lung fibroblast cells (HELs) were isolated from postmortem embryo lung tissue. The original source of the anonymized tissues was Zhongnan Hospital of Wuhan University (China). The cell isolation procedures and research plans were approved by the Institutional Review Board (IRB) (WIVH10201202) according to the Guidelines for Biomedical Research Involving Human Subjects at Wuhan Institute of Virology, Chinese Academy of Sciences. The need for written or oral consents was waived by the IRB (53).

Cells and cell culture. HELs were isolated and maintained as described previously (53). HELF, kindly provided by Dr. Jason J. Chen at Columbia University, are human embryonic lung fibroblasts that have been retrovirally transduced with human telomerase (hTERT). Clonal cell lines isolated from HELFs that were transduced with WDR5 shRNA (KD) and scrambled shRNA (Ctl) were described previously (47). Both HELs and HELF were cultured in Minimum Essential Medium (MEM, Cat.#41500-034, Thermo Fisher) supplemented with 10% fetal bovine serum (FBS, Cat.#10099-141, Thermo Fisher) and penicillin-streptomycin (100 U/ml and 100 μg/ml, respectively; Cat.#15140-122, Thermo Fisher). Human embryonic kidney 293T cells (HEK293T) were purchased from ATCC (CRL-11268) and cultured in Dulbecco's Modified Eagle Medium (DMEM; Cat.#11995-123, Thermo Fisher) supplemented with 10% FBS and penicillin-streptomycin, as above. Cells were cultured at 37 °C in a humidified atmosphere containing 5% CO_2.

Viruses. HCMV Towne strain (ATCC-VR 977) was used in this study. HSV-1 strain H129 expressing GFP was previously constructed by our laboratory (54). VZV Oka

441 strain expressing GFP (55) was a gift from Dr. Hua Zhu, Rutgers-New Jersey Medical
442 School, and MCMV strain K181 was a gift from Qiyi Tang, Howard University
443 College of Medicine, USA. GFP-expressing AdV and AcMNPV were provided by Dr.
444 Zhengli Shi and Zhihong Hu, Wuhan Institute of Virology, Chinese Academy of
445 Sciences, respectively.
446
447 **Plasmid construction.** Primers used for plasmid construction are shown in Table 1.
448 WDR5 cDNA (GenBank #NM_017588) was derived by reverse transcription as
449 described previously (47). The cDNA was PCR amplified then cloned into either
450 *Eco*RI/*Xho*I-restricted pCMV-HA to generate plasmid HA-WDR5 or into
451 *Xba*I/*EcoR*I-restricted pCDH-Flag to generate Flag-WDR5. The *UL83* ORF encoding
452 pp65 and *IRS1* ORF encoding pIRS1 were PCR amplified from Towne-BAC genome
453 (56) and cloned into *Bam*HI/*Kpn*I-restricted pXJ40-Flag to generate plasmid Flag-
454 pp65 and Flag-pIRS1, respectively. The *UL99* ORF encoding pp28 was PCR
455 amplified and cloned into *Bam*HI/*Xba*I-restricted pcDNA3.1-V5/6×His to generate
456 plasmid pp28-6×his. The *UL86* ORF encoding MCP and *UL32* ORF encoding pp150
457 were amplified from Towne-BAC genome (56) and inserted into a vector with 6×Myc
458 by cloning recombination (ClonExpress II One Step Cloning Kit, Cat.#C112,
459 Vazyme). The *TRS1* ORF encoding pTRS1 fused with a carboxyl-terminal 6×His
460 epitope tag and V5 tag was a gift from Dr. Adam P. Geballe, Fred Hutchinson Cancer
461 Research Center and University of Washington, which have been previously
462 described as pEQ981 (57). All the primers used in this study are listed in Table 1.
463
464 **Transient transfection.** 1.5×10^6 HEK293T cells were seeded into 100-mm dishes.
465 The next day the medium was changed 2h prior to transfection via $Ca_2(PO_4)_2$

precipitation with 10 μg HA-WDR5 along with 10 μg pp28-his, Myc-MCP, Flag-pp65, Myc-pp150, Flag-pIRS1, or pTRS1-V5, as described previously (53). 2×10^6 HELFs were seeded onto coverslips in 12-well plates. Medium was changed at 2h prior to transfection in the next day. Plasmids (1.2 μg for each well) expressing full-length and truncated WDR5 were transfected into HELFs using Lipofectamine 2000 reagent (Cat.#11668-019; Thermo) according to the manufacturer's instructions.

Quantitative reverse transcriptase PCR (qRT-PCR). HELFs were infected at an MOI of 3 and harvested at the indicated times post infection. A total of 1×10^6 cells were used for total RNA extraction using RNAiso Plus reagent (Cat.#9109, TaKaRa), followed by treatment with 10 U of recombinant DNase I (Cat.#2270A, TaKaRa) to remove residual DNA. One μg RNA of each sample was reverse transcribed with a RevertAid H Minus first-strand cDNA synthesis kit (Cat.#K1631, Fermentas) with random primers. Then qPCR was performed on a real-time thermocycler (Bio-Rad; Connect) using SYBR green PCR master mix (Cat.#4309155, Applied Biosystems) in 20 μl reactions for 40 PCR cycles as described previously (58). The PCR primers for WDR5 were: 5'-GGTGGGAAGTGGATTGTGTC-3' and 5'-GCAGCAGAGGCGATGATG-3'. The PCR primers for GAPDH were: 5'-GAGTCAACGGATTTGGTCGT-3' and 5'-GACAAGCTTCCCGTTCTCAG-3'.

IB. Cells were harvested in cell lysis buffer (Cat.#P0013, Beyotime) containing protease inhibitor cocktail (Cat.#04693159001, Roche) and homogenized by ultrasonication. Protein concentrations of lysates were determined by Bradford assay (Cat.#500-0205, Bio-Rad). After boiling with loading buffer, cell lysates containing equal protein amounts were separated by SDS-PAGE and transferred to PVDF

membranes (Cat.#ISEQ00010, Millipore). Membranes were sequentially probed with primary antibodies and appropriate peroxidase-conjugated secondary antibodies. All antibodies used for IB are listed in Table 2. The viral antibodies for IE1 (59), pUL48 (60), pIRS1 (61), pTRS1 (61) and MCP (62) and mIE1 (63) were described previously. Blots were developed using the SuperSignal West Femto Chemiluminescent Substrate (Cat.#34095, Thermo Fisher), signals were detected using a FluorChem HD2 System (Alpha Innotech), and quantification was performed using ImageJ software (NIH).

IP. HEL cells were mock infected or infected with HCMV strain Towne at an MOI of 3 and harvested at 72 hpi. Cells were lysed in IP lysis buffer (Cat.#P0013, Beyotime) for 1h at 4 °C then centrifuged at 120,000 × g for 5 min to remove cell debris. Samples were mock treated or nuclease treated by incubation with 10 mM $MgCl_2$, 100 µg/ ml Dnase I (Cat.#2270A, TaKaRa) and 100 µg/ml Rnase A (Cat.#AC118, OMEGA) for 1 h at 37 °C. IP was performed by incubation of the resulting lysates overnight at 4 °C with mouse monoclonal anti-Flag antibody (Cat.# F3165, Sigma) or with normal mouse IgG (Cat.#A7028, Beyotime). Protein A+G agarose beads (Cat.#P2012, Beyotime) were added and incubated for 3 h at 4 °C and then washed five times with lysis buffer. Loading buffer was added and samples were boiled for 5 min before separation by SDS-PAGE followed by IB for detection of WDR5, pp65, or pp28, as described above.

IFA. HELFs or HFFs were seeded onto coverslips and after attachment infected with HCMV at an MOI of 3. Coverslips were collected at the indicated times post infection and fixed with 4% paraformaldehyde. Target proteins were detected by incubation

with primary antibodies and appropriate secondary antibodies, as listed in Table 2, and as described previously (47). Nuclei were counterstained with DAPI (Cat.#D9542, Sigma). Images were obtained using a UltraVIEW VoX (Perkin Elmer) spinning disk laser confocal scanning microscope. 3D z-axis image stacks were acquired with 0.2-µm spacing and 3D modeling was performed using Volocity 5.5 software (Perkin Elmer). Images were median-filtered to reduce noise and contrast was enhanced to improve resolution.

Cytosolic and nuclear fractionation. HELFs were mock infected or infected with HCMV at an MOI of 3, harvested at 72 hpi, and fractionated using the Qproteome Cell Compartment kit (Cat.#37502, Qiagen) as described previously (64). Fractions were analyzed by IB using GAPDH and Lamin B1 antibodies to confirm separation of cytosolic and nuclear fractions, respectively.

Quantitation of viral genome copy number. Genomic DNA from each fraction were analyzed by qPCR to quantitate viral DNAs using HCMV UL83 primers as described previously (53). Means and standard deviations (SD) from at least three independent experiments were calculated.

Virus particles and capsid purification. HELs were infected with HCMV at an MOI of 0.02 and harvested after CPE reached 100%. Culture medium was collected and clarified by centrifugation at 2,000 × *g* for 10 min. Virus particles were pelleted from the supernatants at 100,000 × *g* for 2 h at 4 °C in an SW 32Ti rotor using a Beckman Optima™ L-100 XP Ultracentrifuge. The pellet was resuspended and layered onto an iodixanol gradient that was prepared by sequentially layering 800 ul volumes of 50%,

40%, 30%, 20%, and 10% iodixanol (Cat.#D1556, Sigma) in PBS (v/v) followed by incubation overnight 4 °C. Gradients were then centrifuged 100,000 × *g* for 2 h at 4 °C by using an SW 55Ti rotor and Optima™ MAX-XP Ultracentrifuge. The virion-containing band was observed by light-scattering, collected, and stored at -80 °C.

For purification of nuclear capsids, infected HELs were harvested at 48 hpi, cell pellets were washed with 1 × phosphate-buffered saline (PBS) and incubated in NP-40 lysis buffer (0.5% NP-40, 5 M NaCl, 1 M Tris-HCl, pH = 7.0) at 4 °C for 20 min. Nuclei were centrifuged at 2,000 x *g* for 10 min, resuspended in TNE (500 mM NaCl, 10 mM Tris-HCl, 1 mM EDTA, pH = 8.0), sonicated (VCX130, SONICS) at 25% amplitude for 18 s (3s on, 3s off), and centrifuged at 2,000 x *g* for 10 min. This step was repeated once and combined supernatants were centrifuged at 10,000 x *g* for 20 min at 4°C to remove cell debris. Supernatants containing capsids were subjected to iodixanol density gradient centrifugation described above. Capsids were observed as light-scattering bands, collected, and stored at -80 °C.

Transmission electron microscopy (TEM). HELFs (Ctl) and the WDR knockdown HELFs (KD) were infected with HCMV at an MOI of 0.5 and harvested at 120 hpi. Cells were fixed with 2.5% (W/V) glutaraldehyde for 1 h at room temperature then treated with 1% osmium tetroxide and dehydrated through a graded series of ethanol concentrations (from 30 to 100%) and embedding with an Embed 812 kit (Electron Microscopy Sciences, Fort Washington, PA). Ultrathin sections (60 to 80 nm) of embedded specimens were prepared and deposited onto formvar-coated copper grids (200-mesh), stained with 2% (W/V) phosphotungstic acid (PTA, pH 6.8), and observed under a Tecnai transmission electron microscope (FEI) operated at 200 kV as described previously (47).

566

567 **Immuno-electron microscopy.** Purified virions were mock treated or treated with 2%
568 Triton X-100, then adsorbed onto carbon-coated nickel 150 mesh grids for 2 h at room
569 temperature and blocked with 5% goat serum albumin. Grids were incubated with
570 antibodies to WDR5, gB, pp28, or normal mouse IgG overnight at 4 °C in a
571 humidified chamber. Grids were washed three times for 1 min with PBS and then
572 incubated for 30 min at room temperature with 10-nm colloidal gold-affiniPure goat
573 anti-mouse IgG. Grids were washed once with PBS and once with water, then stained
574 with 2% (w/v) phosphotungstic acid for 30 s. Grids were observed using a Tecnai G^2
575 20 TWIN transmission electron microscope (FEI) operated at 200 kV.

576

577 **LC-MS/MS analysis.** LC-MS/MS analysis was performed on a Q Exactive mass
578 spectrometer (Thermo Scientific) that is coupled to Easy nLC (Proxeon Biosystems,
579 now Thermo Fisher Scientific) for 60 min. The mass spectrometer was operated in
580 positive ion mode. MS data was acquired using a data-dependent top 10 method
581 dynamically choosing the most abundant precursor ions from the survey scan (300–
582 1800 m/z) for HCD fragmentation. Automatic gain control (AGC) target was set to
583 3e6, and maximum inject time to 10 ms. Dynamic exclusion duration was 40.0 s.
584 Survey scans were acquired at a resolution of 70,000 at m/z 200 and resolution for
585 HCD spectra was set to 17,500 at m/z 200. Isolation width was 2 m/z. Normalized
586 collision energy was 30 eV and the underfill ratio, which specifies the minimum
587 percentage of the target value likely to be reached at maximum fill time, was defined
588 as 0.1%. The instrument was run with peptide recognition mode enabled.

589

590 **Statistical analyses.** Data were analyzed by chi-square or one-way ANOVA, as
591 appropriate, using SPSS software (version 18.0; SPSS). Results were shown as means
592 ± one standard deviation from three independent experiments. A value of $P < 0.05$
593 was considered significant.

References

1. **Cobbs CS, Harkins L, Samanta M, Gillespie GY, Bharara S, King PH, Nabors LB, Cobbs CG, Britt WJ.** 2002. Human cytomegalovirus infection and expression in human malignant glioma. Cancer Res **62:**3347-3350.
2. **Wen L, Qiu Y, Cheng S, Jiang X, Ma YP, Fang W, Wang W, Cui J, Ruan Q, Zhao F, Hu F, Luo MH.** 2018. Serologic and viral genome prevalence of HSV, EBV, and HCMV among healthy adults in Wuhan, China. J Med Virol **90:**571-581.
3. **Jean Beltran PM, Cristea IM.** 2014. The life cycle and pathogenesis of human cytomegalovirus infection: lessons from proteomics. Expert Rev Proteomics **11:**697-711.
4. **Tandon R, Mocarski ES.** 2012. Viral and host control of cytomegalovirus maturation. Trends Microbiol **20:**392-401.
5. **Eddleston M, Peacock S, Juniper M, Warrell D.** 1997. Severe cytomegalovirus infection in immunocompetent patients. Clinical infectious diseases **24:**52-56.
6. **Ho M.** 1990. Epidemiology of cytomegalovirus infections. Review of Infectious Diseases **12:**S701-S710.
7. **Söderberg-Nauclér C, Fish KN, Nelson JA.** 1997. Reactivation of latent human cytomegalovirus by allogeneic stimulation of blood cells from healthy donors. Cell **91:**119-126.
8. **Arizaheredia EJ, Nesher L, Chemaly RF.** 2014. Cytomegalovirus diseases after hematopoietic stem cell transplantation: A mini-review. Cancer Lett **342:**1-8.
9. **Dominietto A, Raiola AM, Van Lint MT, Lamparelli T, Gualandi F, Berisso G, Bregante S, Frassoni F, Casarino L, Verdiani S.** 2001. Factors influencing haematological recovery after allogeneic haemopoietic stem cell transplants : graft-versus-host disease, donor type, cytomegalovirus infections and cell dose. Br J Haematol **112:**219-227.
10. **Focosi D, Sordi E, Papineschi F, Benedetti E, Galimberti S, Petrini M.** 2009. Fatal ongoing human cytomegalovirus reactivation during high-dose melphalan and autologous stem cell transplantation†. J Med Virol **81:**857-860.
11. **Streblow DN, Orloff SL, Nelson JA.** 2007. Acceleration of allograft failure by cytomegalovirus. Curr Opin Immunol **19:**577-582.
12. **Han XY.** 2007. Epidemiologic analysis of reactivated cytomegalovirus antigenemia in patients with cancer. J Clin Microbiol **45:**1126-1132.
13. **Boppana S, Britt WJ, Pass RF.** 1997. Progressive and fluctuating sensorineural hearing loss in children with asymptomatic congenital cytomegalovirus infection. Journal of Pediatrics **130**.
14. **Williamson WD, Demmler GJ, Percy AK, Catlin FI.** 1992. Progressive hearing loss in infants with asymptomatic congenital cytomegalovirus infection. Pediatrics **90:**862-866.
15. **Swanson EC, Schleiss MR.** 2013. Congenital cytomegalovirus infection: new prospects for prevention and therapy. Pediatr Clin North Am **60:**335-349.
16. **Kawai K, Itoh H.** 2018. Congenital Cytomegalovirus Infection. N Engl J Med **379:**e21.
17. **Alwine J.** 2012. The Human Cytomegalovirus Assembly Compartment: A Masterpiece of Viral Manipulation of Cellular Processes That Facilitates Assembly and Egress. PLoS Pathog **8:**e1002878.

18. **Sanchez V, Greis KD, Sztul E, Britt WJ.** 2000. Accumulation of virion tegument and envelope proteins in a stable cytoplasmic compartment during human cytomegalovirus replication: characterization of a potential site of virus assembly. Journal of virology **74:**975-986.
19. **Das S, Vasanji A, Pellett PE.** 2007. Three-dimensional structure of the human cytomegalovirus cytoplasmic virion assembly complex includes a reoriented secretory apparatus. J Virol **81:**11861-11869.
20. **Seo JY, Britt WJ.** 2007. Cytoplasmic envelopment of human cytomegalovirus requires the postlocalization function of tegument protein pp28 within the assembly compartment. J Virol **81:**6536-6547.
21. **Das S, Ortiz DA, Gurczynski SJ, Khan F, Pellett PE.** 2014. Identification of human cytomegalovirus genes important for biogenesis of the cytoplasmic virion assembly complex. J Virol **88:**9086-9099.
22. **Goulidaki N, Alarifi S, Alkahtani SH, Al-Qahtani A, Spandidos DA, Stournaras C, Sourvinos G.** 2015. RhoB is a component of the human cytomegalovirus assembly complex and is required for efficient viral production. Cell Cycle **14:**2748-2763.
23. **Xie M, Xuan B, Shan J, Pan D, Sun Y, Shan Z, Zhang J, Yu D, Li B, Qian Z.** 2015. Human cytomegalovirus exploits interferon-induced transmembrane proteins to facilitate morphogenesis of the virion assembly compartment. J Virol **89:**3049-3061.
24. **Bughio F, Umashankar M, Wilson J, Goodrum F.** 2015. Human Cytomegalovirus UL135 and UL136 Genes Are Required for Postentry Tropism in Endothelial Cells. J Virol **89:**6536-6550.
25. **Hook LM, Grey F, Grabski R, Tirabassi R, Doyle T, Hancock M, Landais I, Jeng S, McWeeney S, Britt W, Nelson JA.** 2014. Cytomegalovirus miRNAs target secretory pathway genes to facilitate formation of the virion assembly compartment and reduce cytokine secretion. Cell Host Microbe **15:**363-373.
26. **Cruz L, Streck NT, Ferguson K, Desai T, Desai D, Amin S, Buchkovich NJ.** 2017. Potent Inhibition of Human Cytomegalovirus by Modulation of Cellular SNARE Syntaxin 5. Journal of Virology **91**.
27. **Buchkovich NJ, Maguire TG, Alwine JC.** 2010. Role of the endoplasmic reticulum chaperone BiP, SUN domain proteins, and dynein in altering nuclear morphology during human cytomegalovirus infection. J Virol **84:**7005-7017.
28. **Buchkovich NJ, Maguire TG, Paton AW, Paton JC, Alwine JC.** 2009. The endoplasmic reticulum chaperone BiP/GRP78 is important in the structure and function of the human cytomegalovirus assembly compartment. J Virol **83:**11421-11428.
29. **Indran SV, Ballestas ME, Britt WJ.** 2010. Bicaudal D1-dependent trafficking of human cytomegalovirus tegument protein pp150 in virus-infected cells. J Virol **84:**3162-3177.
30. **Krzyzaniak MA, Mach M, Britt WJ.** 2009. HCMV-encoded glycoprotein M (UL100) interacts with Rab11 effector protein FIP4. Traffic **10:**1439-1457.
31. **Varnum SM, Streblow DN, Monroe ME, Smith P, Auberry KJ, Pasa-Tolic L, Wang D, Camp DG, 2nd, Rodland K, Wiley S, Britt W, Shenk T, Smith RD, Nelson JA.** 2004. Identification of proteins in human cytomegalovirus (HCMV) particles: the HCMV proteome. J Virol **78:**10960-10966.
32. **Abraham E, Pantoja M, Kucherenko MM, Yatsenko AS, Shcherbata HR, Fischer KA, Maksymiv DV, Chernyk YI, Ruohola-Baker H.** 2008.

694 Genetic Modifier Screens Reveal New Components that Interact with the
695 Drosophila Dystroglycan-Dystrophin Complex. PLoS ONE **3:**e2418.
696 33. **Dias J, Van Nguyen N, Georgiev P, Gaub A, Brettschneider J, Cusack**
697 **S, Kadlec J, Akhtar A.** 2014. Structural analysis of the
698 KANSL1/WDR5/KANSL2 complex reveals that WDR5 is required for efficient
699 assembly and chromatin targeting of the NSL complex. Genes Dev **28:**929-
700 942.
701 34. **Cho YW, Hong T, Hong S, Guo H, Yu H, Kim D, Guszczynski T,**
702 **Dressler GR, Copeland TD, Kalkum M, Ge K.** 2007. PTIP associates with
703 MLL3- and MLL4-containing histone H3 lysine 4 methyltransferase complex. J
704 Biol Chem **282:**20395-20406.
705 35. **Song JJ, Kingston RE.** 2008. WDR5 interacts with mixed lineage leukemia
706 (MLL) protein via the histone H3-binding pocket. J Biol Chem **283:**35258-
707 35264.
708 36. **Mo R, Rao SM, Zhu YJ.** 2006. Identification of the MLL2 complex as a
709 coactivator for estrogen receptor alpha. J Biol Chem **281:**15714-15720.
710 37. **Dharmarajan V, Lee JH, Patel A, Skalnik DG, Cosgrove MS.** 2012.
711 Structural basis for WDR5 interaction (Win) motif recognition in human SET1
712 family histone methyltransferases. J Biol Chem **287:**27275-27289.
713 38. **Chen X, Xie W, Gu P, Cai Q, Wang B, Xie Y, Dong W, He W, Zhong G,**
714 **Lin T, Huang J.** 2015. Upregulated WDR5 promotes proliferation, self-
715 renewal and chemoresistance in bladder cancer via mediating H3K4
716 trimethylation. Sci Rep **5:**8293.
717 39. **Wu MZ, Tsai YP, Yang MH, Huang CH, Chang SY, Chang CC, Teng SC,**
718 **Wu KJ.** 2011. Interplay between HDAC3 and WDR5 is essential for hypoxia-
719 induced epithelial-mesenchymal transition. Mol Cell **43:**811-822.
720 40. **Wysocka J, Swigut T, Milne TA, Dou Y, Zhang X, Burlingame AL,**
721 **Roeder RG, Brivanlou AH, Allis CD.** 2005. WDR5 associates with histone
722 H3 methylated at K4 and is essential for H3 K4 methylation and vertebrate
723 development. Cell **121:**859-872.
724 41. **Zhu ED, Demay MB, Gori F.** 2008. Wdr5 is essential for osteoblast
725 differentiation. J Biol Chem **283:**7361-7367.
726 42. **Kulkarni SS, Griffin JN, Date PP, Liem KF, Jr., Khokha MK.** 2018.
727 WDR5 Stabilizes Actin Architecture to Promote Multiciliated Cell Formation.
728 Dev Cell **46:**595-610 e593.
729 43. **Ang YS, Tsai SY, Lee DF, Monk J, Su J, Ratnakumar K, Ding J, Ge Y,**
730 **Darr H, Chang B, Wang J, Rendl M, Bernstein E, Schaniel C,**
731 **Lemischka IR.** 2011. Wdr5 mediates self-renewal and reprogramming via
732 the embryonic stem cell core transcriptional network. Cell **145:**183-197.
733 44. **Yang YW, Flynn RA, Chen Y, Qu K, Wan B, Wang KC, Lei M, Chang HY.**
734 2014. Essential role of lncRNA binding for WDR5 maintenance of active
735 chromatin and embryonic stem cell pluripotency. Elife **3:**e02046.
736 45. **Wang YY, Liu LJ, Zhong B, Liu TT, Li Y, Yang Y, Ran Y, Li S, Tien P,**
737 **Shu HB.** 2010. WDR5 is essential for assembly of the VISA-associated
738 signaling complex and virus-triggered IRF3 and NF-kappaB activation. PNAS
739 **107:**815-820.
740 46. **Ma D, George CX, Nomburg JL, Pfaller CK, Cattaneo R, Samuel CE.**
741 2018. Upon Infection, Cellular WD Repeat-Containing Protein 5 (WDR5)
742 Localizes to Cytoplasmic Inclusion Bodies and Enhances Measles Virus
743 Replication. J Virol **92:**e01726-01717.
744 47. **Yang B, Liu XJ, Yao Y, Jiang X, Wang XZ, Yang H, Sun JY, Miao Y,**
745 **Wang W, Huang ZL, Wang Y, Tang Q, Rayner S, Britt WJ, McVoy MA,**

Luo MH, Zhao F. 2018. WDR5 Facilitates Human Cytomegalovirus Replication by Promoting Capsid Nuclear Egress. J Virol **92:**e00207-00218.

48. **Oakley BR, Oakley CE, Yoon Y, Jung MK.** 1990. γ-Tubulin is a component of the spindle pole body that is essential for microtubule function in Aspergillus nidulans. Cell **61:**1289-1301.

49. **Vasquez R, Howell B, Yvon A, Wadsworth P, Cassimeris L.** 1997. Nanomolar concentrations of nocodazole alter microtubule dynamic instability in vivo and in vitro. Molecular Biology of the Cell **8**.

50. **Li W, Avey D, Fu B, Wu JJ, Ma S, Liu X, Zhu F.** 2016. Kaposi's Sarcoma-Associated Herpesvirus Inhibitor of cGAS (KicGAS), Encoded by ORF52, Is an Abundant Tegument Protein and Is Required for Production of Infectious Progeny Viruses. J Virol **90:**5329-5342.

51. **Shaw ML, Stone KL, Colangelo CM, Gulcicek EE, Palese P.** 2008. Cellular proteins in influenza virus particles. PLoS Pathog **4:**e1000085.

52. **Dell'Oste V, Gatti D, Gugliesi F, De Andrea M, Bawadekar M, Lo Cigno I, Biolatti M, Vallino M, Marschall M, Gariglio M, Landolfo S.** 2014. Innate nuclear sensor IFI16 translocates into the cytoplasm during the early stage of in vitro human cytomegalovirus infection and is entrapped in the egressing virions during the late stage. J Virol **88:**6970-6982.

53. **Fu YR, Liu XJ, Li XJ, Shen ZZ, Yang B, Wu CC, Li JF, Miao LF, Ye HQ, Qiao GH, Rayner S, Chavanas S, Davrinche C, Britt WJ, Tang Q, McVoy M, Mocarski E, Luo MH.** 2015. MicroRNA miR-21 attenuates human cytomegalovirus replication in neural cells by targeting Cdc25a. J Virol **89:**1070-1082.

54. **Zeng WB, Jiang HF, Gang YD, Song YG, Shen ZZ, Yang H, Dong X, Tian YL, Ni RJ, Liu Y, Tang N, Li X, Jiang X, Gao D, Androulakis M, He XB, Xia HM, Ming YZ, Lu Y, Zhou JN, Zhang C, Xia XS, Shu Y, Zeng SQ, Xu F, Zhao F, Luo MH.** 2017. Anterograde monosynaptic transneuronal tracers derived from herpes simplex virus 1 strain H129. Mol Neurodegener **12:**38.

55. **Jiang HF, Wang W, Jiang X, Zeng WB, Shen ZZ, Song YG, Yang H, Liu XJ, Dong X, Zhou J, Sun JY, Yu FL, Guo L, Cheng T, Rayner S, Zhao F, Zhu H, Luo MH.** 2017. ORF7 of Varicella-Zoster Virus Is Required for Viral Cytoplasmic Envelopment in Differentiated Neuronal Cells. J Virol **91**.

56. **Marchini A, Liu H, Zhu H.** 2001. Human cytomegalovirus with IE-2 (UL122) deleted fails to express early lytic genes. J Virol **75:**1870-1878.

57. **Hakki M, Geballe AP.** 2005. Double-stranded RNA binding by human cytomegalovirus pTRS1. J Virol **79:**7311-7318.

58. **Fu Y-R, Liu X-J, Li X-J, Shen Z-z, Yang B, Wu C-C, Li J-F, Miao L-F, Ye H-Q, Qiao G-H.** 2015. MicroRNA miR-21 attenuates human cytomegalovirus replication in neural cells by targeting Cdc25a. Journal of virology **89:**1070-1082.

59. **Plachter B, Britt W, Vornhagen R, Stamminger T, Jahn G.** 1993. Analysis of proteins encoded by IE regions 1 and 2 of human cytomegalovirus using monoclonal antibodies generated against recombinant antigens. Virology **193:**642-652.

60. **Bechtel JT, Shenk T.** 2002. Human Cytomegalovirus UL47 Tegument Protein Functions after Entry and before Immediate-Early Gene Expression. Journal of Virology **76:**1043-1050.

61. **Romanowski MJ, Garrido-Guerrero E, Shenk T.** 1997. pIRS1 and pTRS1 are present in human cytomegalovirus virions. J Virol **71:**5703-5705.

797 62. **Lai L, Britt WJ.** 2003. The Interaction between the Major Capsid Protein and
798 the Smallest Capsid Protein of Human Cytomegalovirus Is Dependent on Two
799 Linear Sequences in the Smallest Capsid Protein. Journal of Virology
800 **77:**2730-2735.
801 63. **Tang Q, Maul GG.** 2003. Mouse cytomegalovirus immediate-early protein 1
802 binds with host cell repressors to relieve suppressive effects on viral
803 transcription and replication during lytic infection. J Virol **77:**1357-1367.
804 64. **Li XJ, Liu XJ, Yang B, Fu YR, Zhao F, Shen ZZ, Miao LF, Rayner S,**
805 **Chavanas S, Zhu H, Britt WJ, Tang Q, McVoy MA, Luo MH.** 2015.
806 Human Cytomegalovirus Infection Dysregulates the Localization and Stability
807 of NICD1 and Jag1 in Neural Progenitor Cells. J Virol **89:**6792-6804.

808

809

FIGURE LEGENDS

Fig 1. Perinuclear relocalization of WDR5 is specifically induced by HCMV and MCMV infection. HELFs (A and C) or NIH3T3 (B) were infected with the indicated viruses at an MOI of 1. At 48 hpi, cells were fixed and stained with antibodies against WDR5(red) and with either HCMV IE1 protein (A) (green) or MCMV mIE1 (green) (B). Infected cells (C) were detected using corresponding GFP-expressing recombinant viruses. All antibodies used in IFA were mouse monoclonal antibodies. Nuclei were counterstained with DAPI (white). M, mock-infected cells; scale bar = 10 μm.

Fig 2. HCMV infection induces re-localization and oligomerization of WDR5. (A) HELFs were mock- (M) or HCMV-infected (V) at an MOI of 3 then processed for immunofluorescence with antibodies against IE1 (green), WDR5 (red), or nuclei (DAPI, white) at the indicated times post infection. Images shown were representative of three independent experiments. All antibodies used in IFA were mouse monoclonal antibodies. Scale bar = 10 μm. (B) Over 100 cells in five representative fields from each independent experiment described in (A) were counted to determine the percentages of infected cells exhibiting diffuse nuclear localization of WDR5 (normal) versus accumulation of WDR5 in perinuclear foci. Data were analyzed using the chi-squared test. N, number counted cells; NS, not significant; ***, $P < 0.001$. (C) HELFs were mock- (M) or HCMV-infected (V) at an MOI of 3. At 96 hpi cytosolic and nuclear fractions were prepared and analyzed by IB for WDR5, pp28, IE1, GAPDH, or Lamin B1. (D) HELFs were mock- or HCMV-infected at an MOI = 1. At 48 hpi, infected cells were treated with DMSO or nuclear export inhibitor Leptomycin B (LMB, 5μM) for 12 h, and were co-stained for WDR5 (red), viral protein pp65 (green)

and nuclei were counterstained with DAPI (white). All antibodies used in IFA were mouse monoclonal antibodies. Scale bar = 10 μm.

Fig 3. WDR5 perinuclear accumulation requires viral replication. HELFs were mock- (M), UV-inactivated HCMV (UV), or live HCMV-infected (V) at an MOI of 3 in the presence of DMSO, GCV (100 μg/ml), or PAA (100 μg/ml). At 72 hpi, samples were collected and analyzed. (A) The upper panel shows protein levels of WDR5 and viral proteins determined by IB with actin as a loading control. The lower panel shows the relative levels of WDR5 protein in infected vs. mock-infected cultures normalized with GAPDH. Data from three independent experiments were analyzed by one-way ANOVA, and the results are presented as averages +/- SD. *, $P < 0.05$; **, $P < 0.01$, NS, no significance. (B) Relative mRNA levels of WDR5. Samples were harvested at the indicated times, and total RNA was isolated. Relative mRNA levels of WDR5 were determined by qRT-PCR; GAPDH is an internal control. Data were normalized to levels in mock-infected cells to provide fold-changes post HCMV infection. (C) Accumulation of WDR5 in perinuclear region. WDR5 perinuclear foci are indicated by white arrows; scale bar = 10 μm.

Fig 4. WDR5 localizes to vAC and MTOC. (A) HELFs were infected with HCMV at an MOI of 3 and at 72 hpi co-stained for WDR5 and markers of cytoskeleton (α-tubulin), centrosome (γ-tubulin), Golgi (58K), or early endosome (EEA1). (B) HELFs were infected for 72 h and then treated with 2 μM NOC for the times indicated prior to staining for WDR5. (C) HCMV-infected HELFs were stained at 96 hpi for WDR5 (red) and co-stained for viral proteins pp28, pp65, or gB (green). Panel below shows a 3D-reconstruction of WDR5 colocalization with gB from the cell shown in the panel

above. Scale bar = 10 μm. (D) WDR5 associated with HCMV capsid protein in vAC. HFFs were infected with HCMV at an MOI of 3 and stained for WDR5 (green), SCP (red), and DNA (blue) at 96 hpi and analyzed with Nikon A1R HD25 confocal system. Top panels show deconvolved single channel maximum intensity z axis projections of a representative cell. Panels below show 3-D reconstructions of deconvolved confocal Z-series images of the vAC. All antibodies used in IFA were mouse monoclonal antibodies, nuclei were counterstained with DAPI. and scale bar = 10 μm.

Fig 5. Knockdown WDR5 altered vAC formation and virion morphogenesis

(A) HELFs were transduced with shRNA to WDR5 (KD) or a scrambled control shRNA (Ctl) as described previously (47). Cells were infected with HCMV at an MOI of 0.5, harvested at 96 hpi, stained for gB with mouse monoclonal antibody, nuclei were counterstained with DAPI, scale bar = 10 μm (Left upper panels). Based on morphology, vACs were classified as regular or irregular, and representative images are shown (a, b, c, and d, Left lower panels). Regular and irregular vACs were quantitated (Right panel). n, number of quantitated infected cells; data were analyzed by chi-squared test. ***, $P < 0.001$.(B) Ctl (a to e) and KD (f to k) cells were infected with HCMV at an MOI of 0.5. At 120hpi, cells were fixed, embedded, sectioned and negative-stained for TEM analysis. Representative images are shown to illustrate the enveloped virions (arrowheads), and nonenveloped capsids (arrows) in the cytoplasm. (C) Quantitation and classification of viral particles. About three hundred total cytoplasmic viral particels were counted. The percentages of normal virions and nonenveloped capsids in each infection are illustrated. Data were analyzed by chi-squared test. n, number of cytoplasmic viral particles counted cells; ***, $P < 0.001$.

Fig 6. Subcellular localization of different WDR5 deletion mutants

(A) Schematic representation of N-terminal Flag-tagged full-length WDR5 and deletion mutants. Flag, Flag tag; L, linker-GAAAAS; NT, N-terminal; WD, WD40-repeat motif. (B) Expression vectors encoding full-length WDR5 or deletion mutants were transfected in HELF cells. At 24 hours post transfection, cells were mock-infected (M) or infected with HCMV (V) at an MOI of 3. At 72 hpi, samples were collected and analyzed by IFA for pp28 (green), Flag (red), or nuclei (DAPI, white). All antibodies used in IFA were mouse monoclonal antibodies. Scale bar = 10 μm.

Fig 7. WDR5 co-purifies with HCMV particles by gradient fractionation. (A) Flow chart illustrating the analysis of particles from mock- or HCMV-infected cultures by iodixanol density gradient centrifugation (see Materials and Methods for details). (B) Gradient fractions derived from mock-infected (M) or infected (V) cultures were analyzed by immune-dot-blot for WDR5, gB, or pUL48. (C) Viral-genome copies in each fraction were determined by qPCR and plotted together with protein levels quantitated using ImageJ software from the dot-blots shown in (B).

Fig 8. WDR5 is present in HCMV virions. (A) Purified HCMV virions were mock treated or treated with 2% Triton X-100 for 1 hour at room temperature then analyzed by iodixanol density gradient centrifugation. Fractions collected from gradients of virions that were mock treated (top) or Triton X-100-treated (bottom), as well as unfractionated lysates from mock- (M) or HCMV-infected (V) HELFs, were analyzed by IB using the indicated antibodies. (B) Mock- or Triton X-100-treated virions were analyzed by immuno-gold electron microscopy using mAbs to gB (a), pp28 (b),

910 WDR5 (c), or normal mouse IgG (d). Samples were negatively stained with
911 phosphotungstic acid and visualized by electron microscopy (25,000 × magnification).
912 (C) HCMV virions were purified as previously described. Nuclei from infected-HELs
913 were prepared at 60 hpi and intracunclear capsids were purified as in described in
914 Materials and Methods. Purified virions and capsids were visualized by electron
915 microscopy. The components (viral proteins and WDR5) were analyzed by IB.
916
917 **Fig 9. WDR5 interacts with MCP, pp150, pp65, pIRS1, and pTRS1.** (A) HELF
918 overexpressing with Flag-tagged WDR5 were mock- (M) or HCMV-infected (V) at
919 an MOI of 3. At 96 hpi lysates were immunoprecipitated by anti-Flag antibody,
920 separated by SDS-PAGE, and stained with Coomassie Brilliant Blue. Four protein
921 species specific to infected cells (red arrows, lane 4) were cut from the gel and
922 combined and analyzed by LC-MS/MS. (B) Spectral counts of identified viral
923 proteins by mass spectrometric analyses are shown. (C-H) HEK293T cells were co-
924 transfected with a plasmid expressing HA-tagged WDR5 (HA-WDR5) along with
925 plasmids expressing His-tagged pp28 (pp28-6×His) (C), Myc-tagged MCP (6×Myc-
926 MCP) (D), Flag-tagged pp65 (Flag-pp65) (E), Myc-tagged pp150 (6×Myc-pp150) (F),
927 Flag-tagged pIRS1 (Flag-IRS1) (G), or V5-tagged pTRS1 (pTRS1-V5) (H). After 48
928 h lysates were immunoprecipitated and then immunoblotted using the indicated
929 antibodies.
930
931 **Fig 10. Working model.** In the nucleus WDR5 facilitates capsid nuclear egress by
932 promoting assembly of the NEC (Yang B, *et al*. J Virol 2018). WDR5 may egress
933 from the nuclei with the capsids and then be transported to the vAC together with

934 capsids and/or tegument proteins (*eg.* pp150 and pp65, *etc*.). In the vAC, WDR5 is

935 incorporated into maturing virions.

FIG1

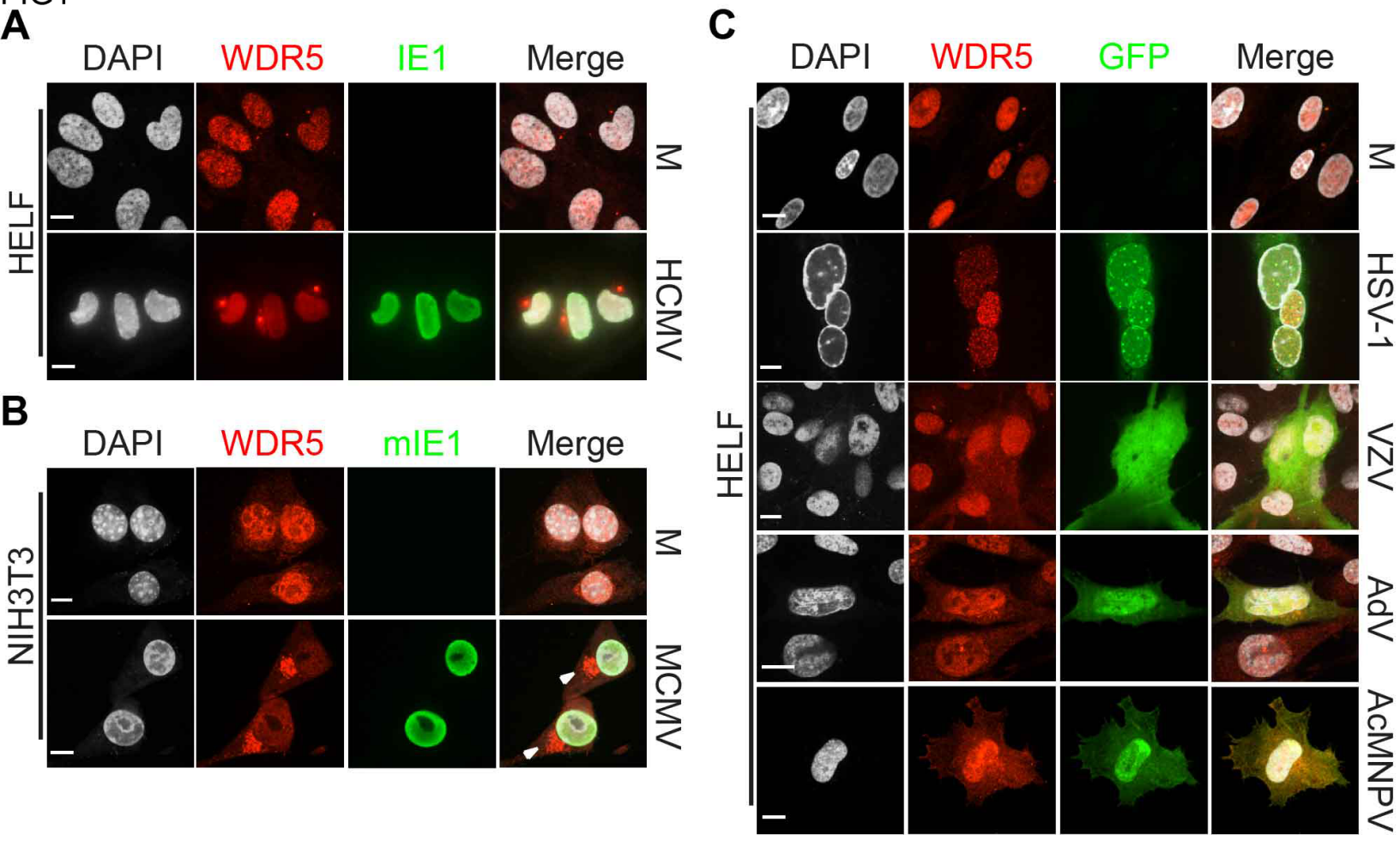
A
DAPI
WDR5
IE1
Merge
HELF
M
HCMV
B
DAPI
WDR5
mIE1
Merge
NIH3T3
M
MCMV
C
DAPI
WDR5
GFP
Merge
HELF
M
HSV-1
VZV
AdV
AcMNPV

FIG2

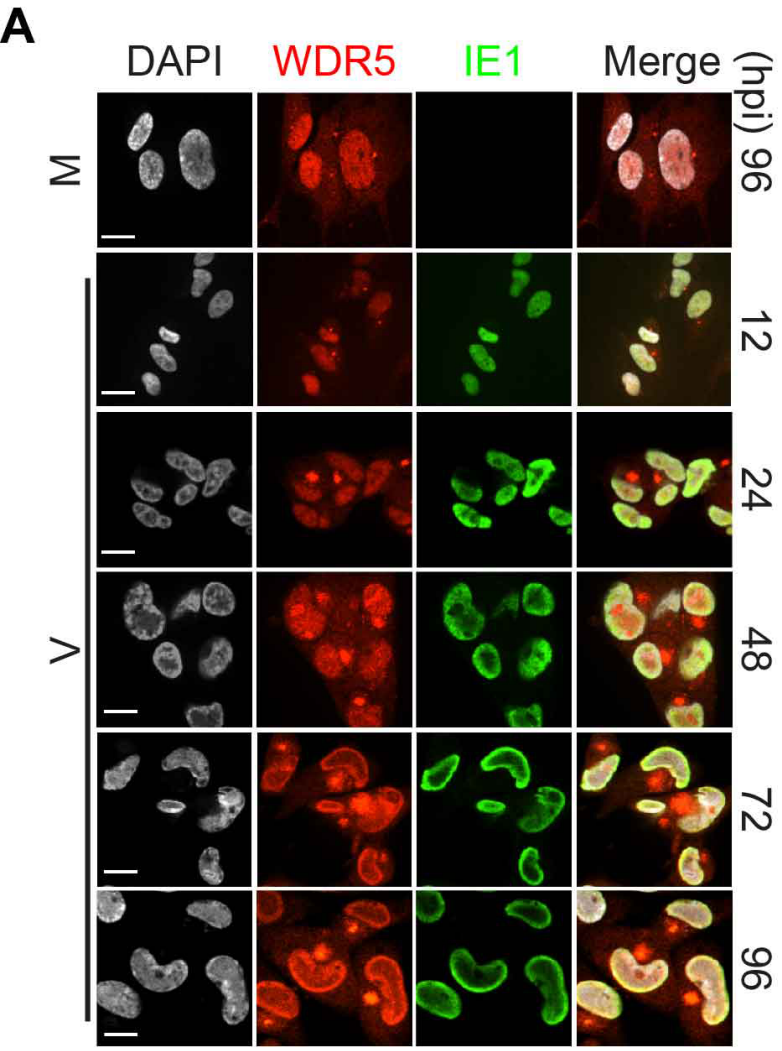
A
DAPI
WDR5
IE1
Merge
(hpi)
M
V
96
12
24
48
72
96

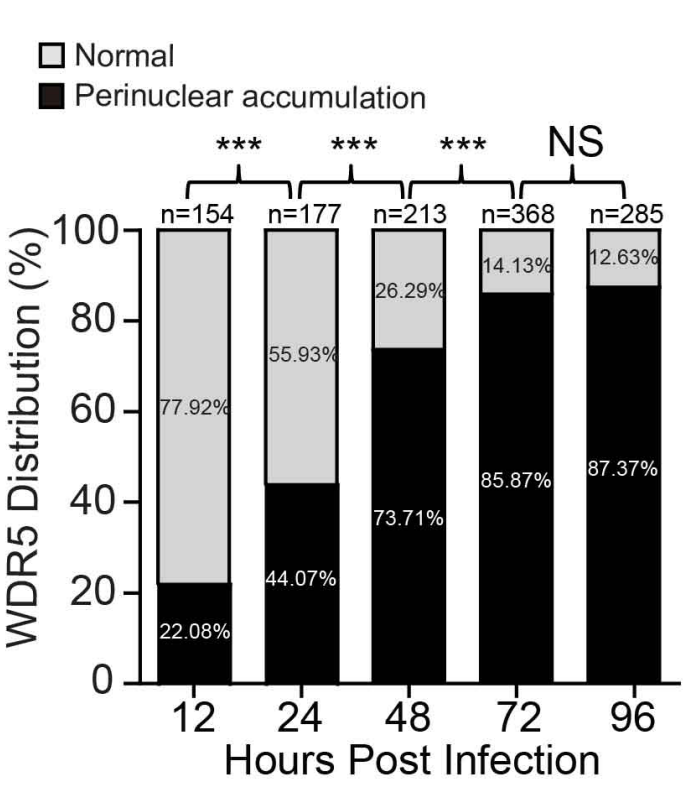
B
Normal
Perinuclear accumulation
***
***
***
NS
n=154
n=177
n=213
n=368
n=285
WDR5 Distribution (%)
100
80
60
40
20
0
77.92%
55.93%
26.29%
14.13%
12.63%
22.08%
44.07%
73.71%
85.87%
87.37%
12
24
48
72
96
Hours Post Infection

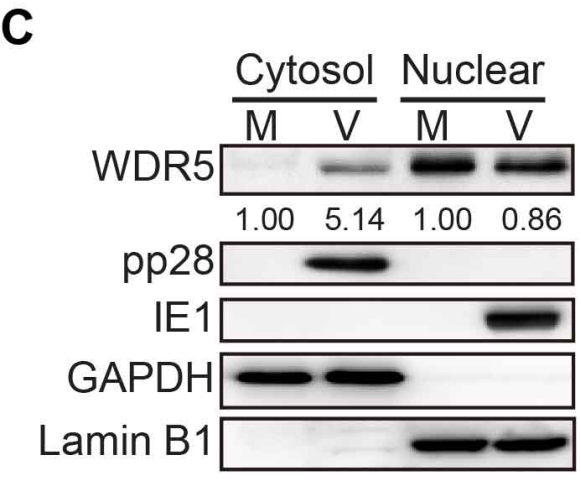
C
Cytosol
Nuclear
M
V
M
V
WDR5
1.00
5.14
1.00
0.86
pp28
IE1
GAPDH
Lamin B1

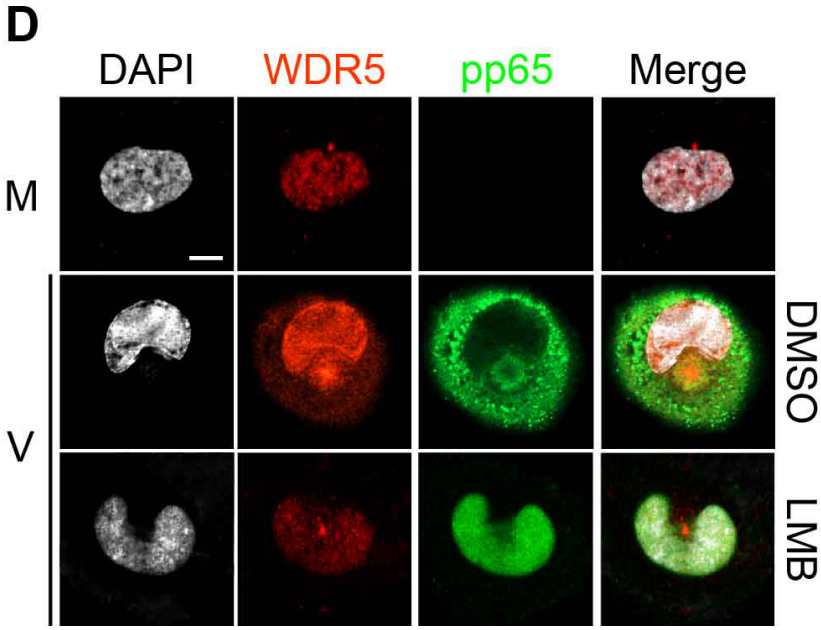
D
DAPI
WDR5
pp65
Merge
M
V
DMSO
LMB

FIG3

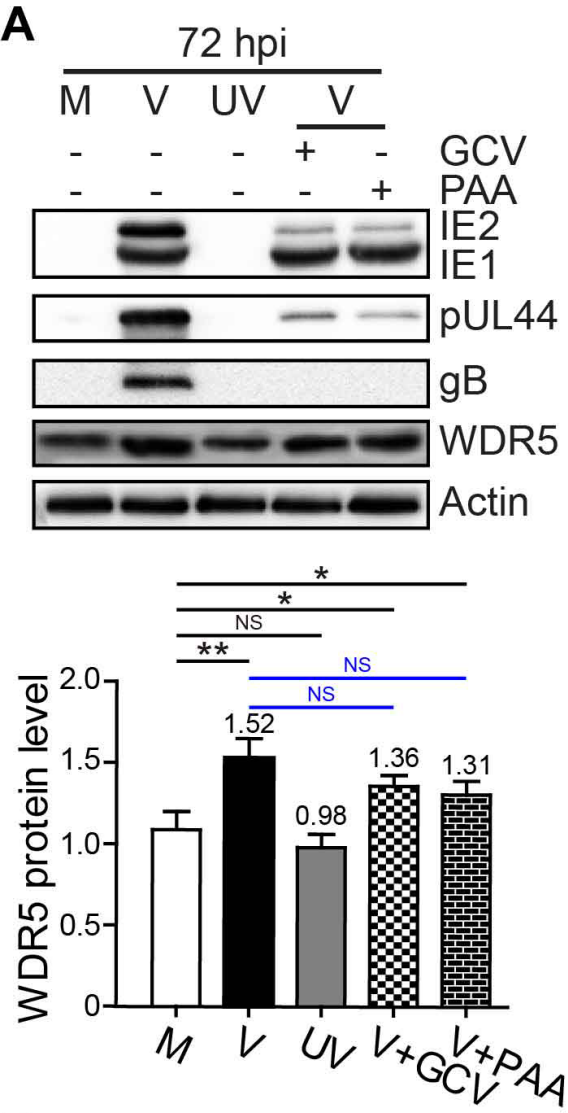
A
72 hpi
M
V
UV
V
GCV
PAA
IE2
IE1
pUL44
gB
WDR5
Actin
WDR5 protein level
1.52
0.98
1.36
1.31
NS
M
V
UV
V+GCV
V+PAA

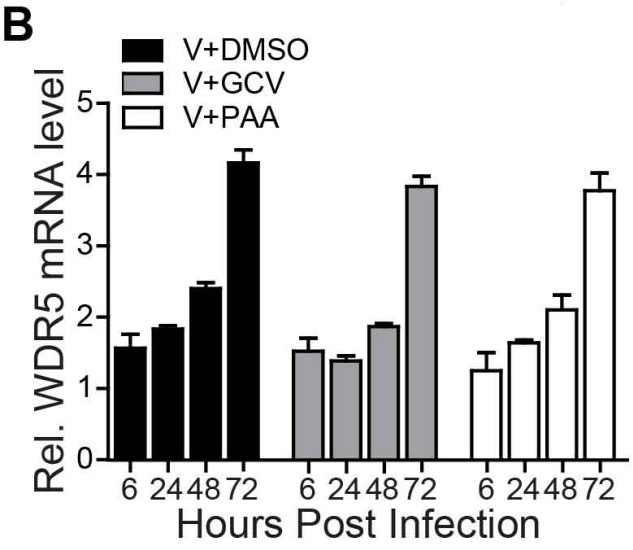
B
V+DMSO
V+GCV
V+PAA
Rel. WDR5 mRNA level
Hours Post Infection

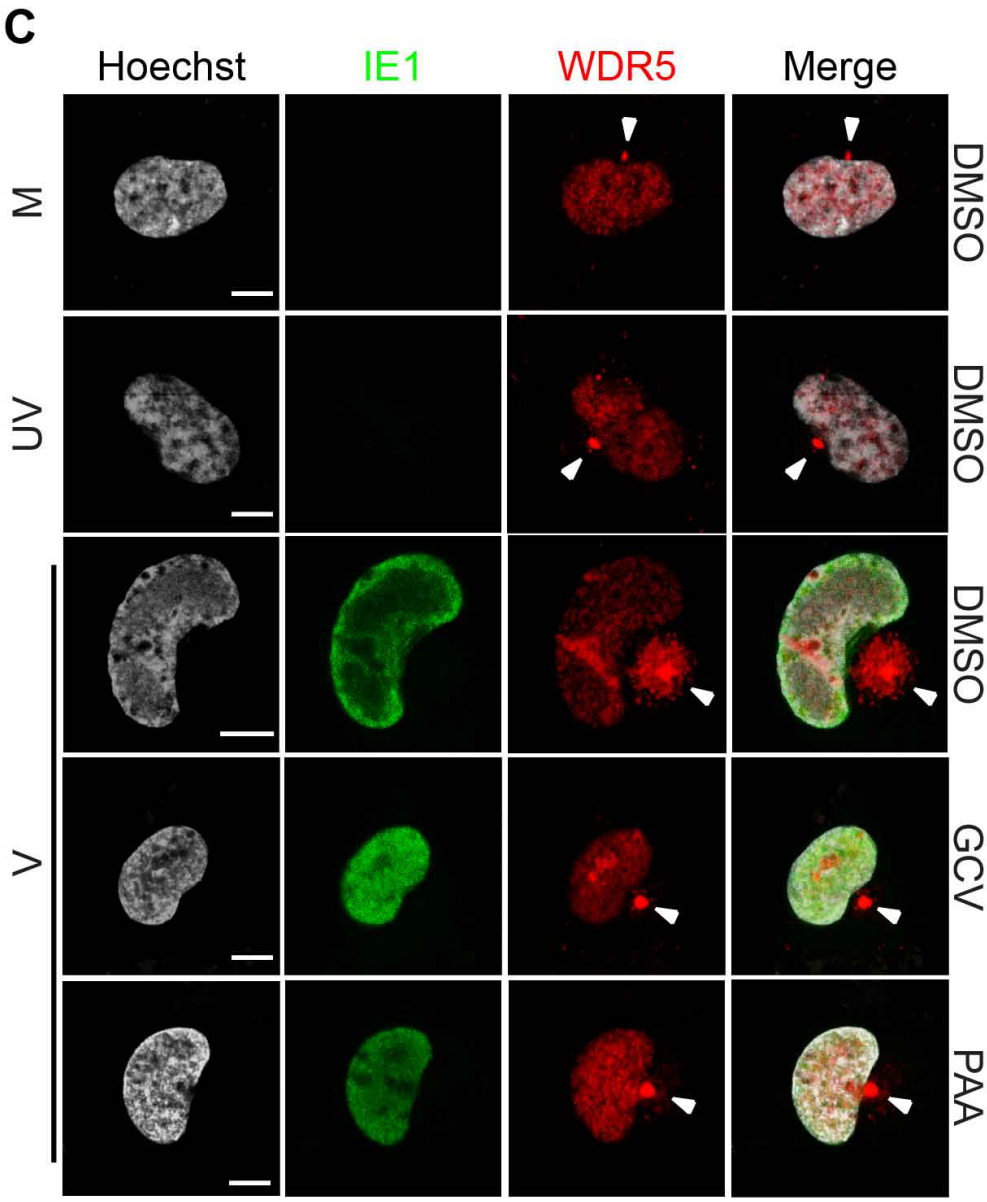
C
Hoechst
IE1
WDR5
Merge
M
UV
V
DMSO
GCV
PAA

FIG4

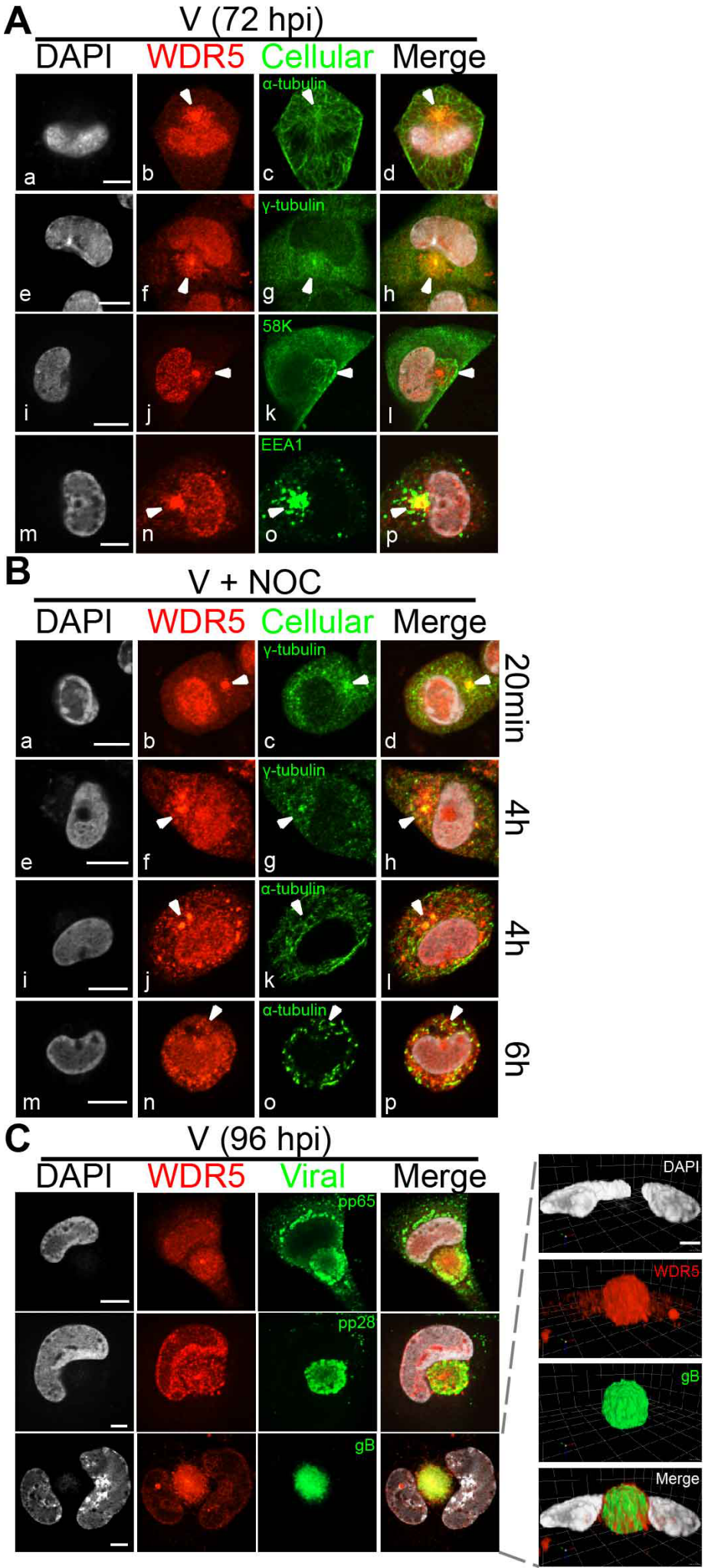
A
V (72 hpi)
DAPI
WDR5
Cellular
Merge
α-tubulin
γ-tubulin
58K
EEA1
B
V + NOC
20min
4h
4h
6h
C
V (96 hpi)
Viral
pp65
pp28
gB
Merge

FIG5

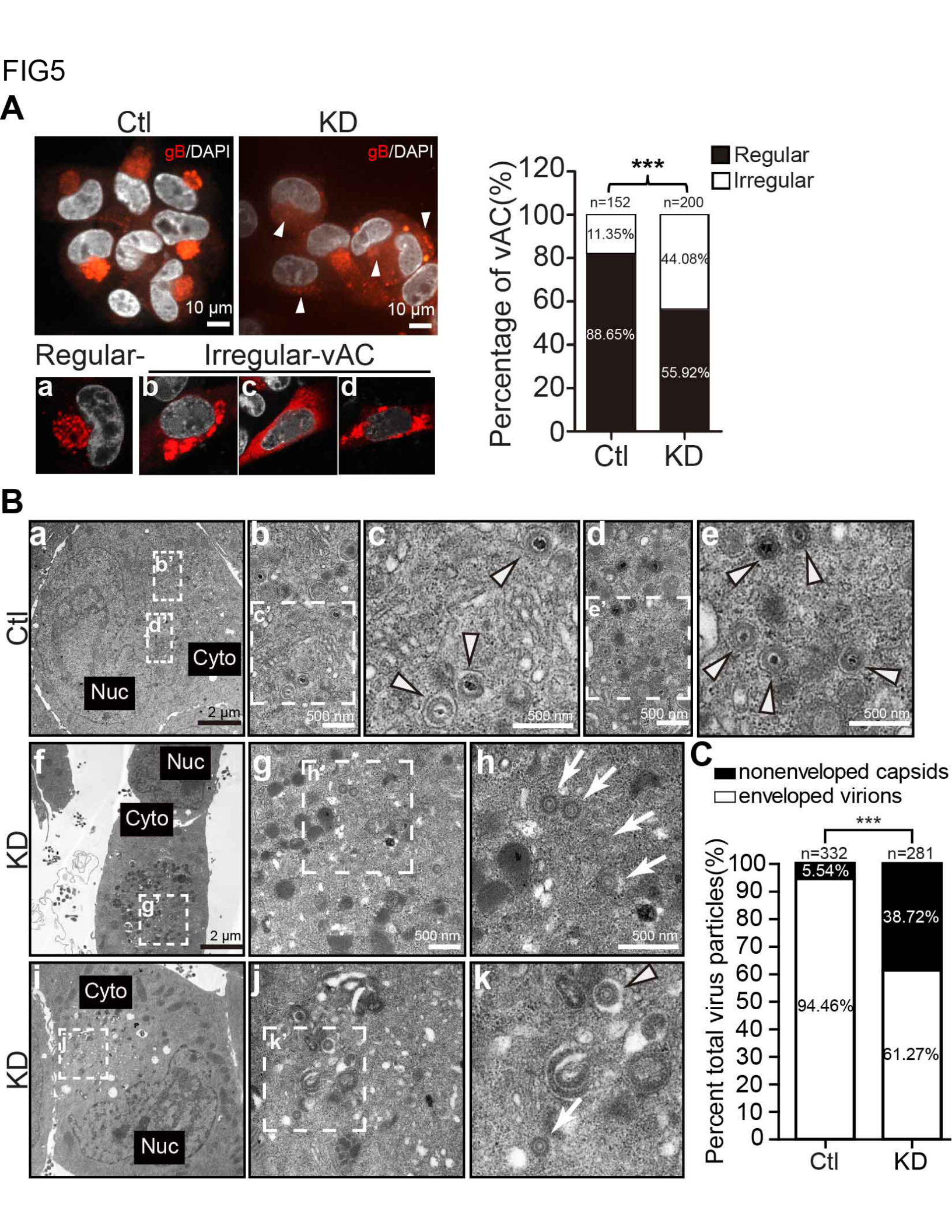
A
Ctl
KD
gB/DAPI
gB/DAPI
10 μm
10 μm
Regular-
Irregular-vAC
a
b
c
d
Regular
Irregular
***
n=152
n=200
11.35%
44.08%
88.65%
55.92%
Percentage of vAC(%)
120
100
80
60
40
20
0
Ctl
KD
B
Ctl
KD
KD
Cyto
Nuc
2 μm
500 nm
C
nonenveloped capsids
enveloped virions
***
n=332
n=281
5.54%
38.72%
94.46%
61.27%
Percent total virus particles(%)
100
90
80
70
60
50
40
30
20
10
0
Ctl
KD

FIG6

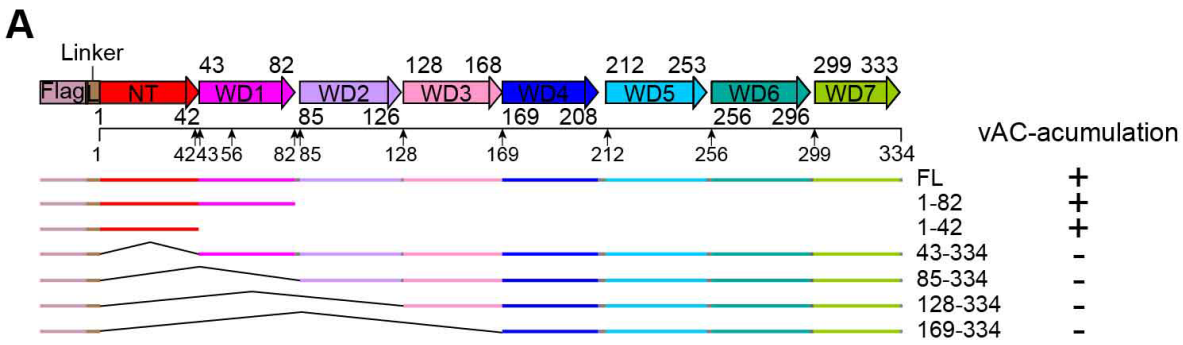
A
Linker
Flag
L
NT
WD1
WD2
WD3
WD4
WD5
WD6
WD7
1
42
43
82
85
126
128
168
169
208
212
253
256
296
299
333
1
42
43
56
82
85
128
169
212
256
299
334
vAC-acumulation
FL +
1-82 +
1-42 +
43-334 -
85-334 -
128-334 -
169-334 -

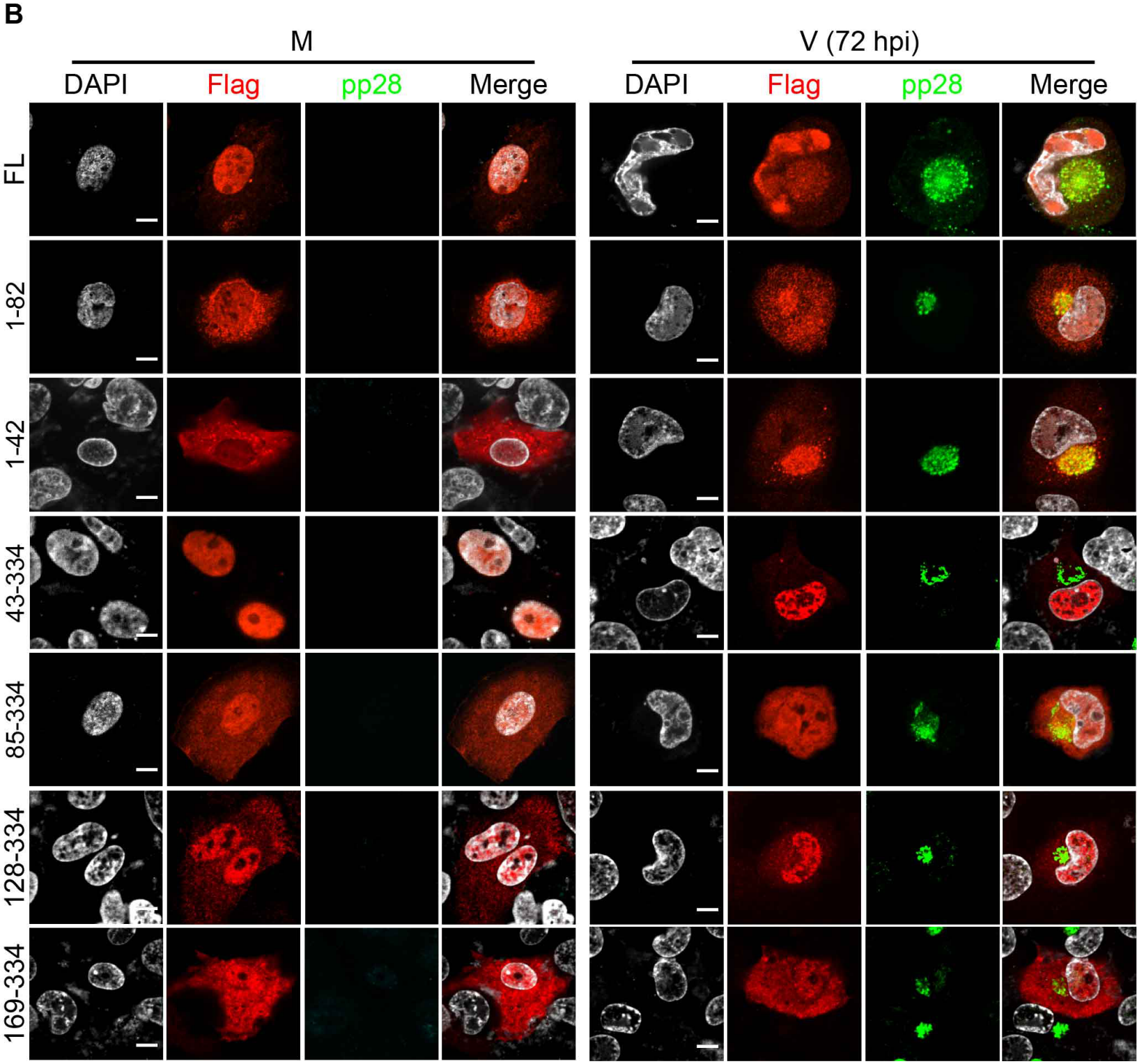
B
M
V (72 hpi)
DAPI
Flag
pp28
Merge
FL
1-82
1-42
43-334
85-334
128-334
169-334

FIG7

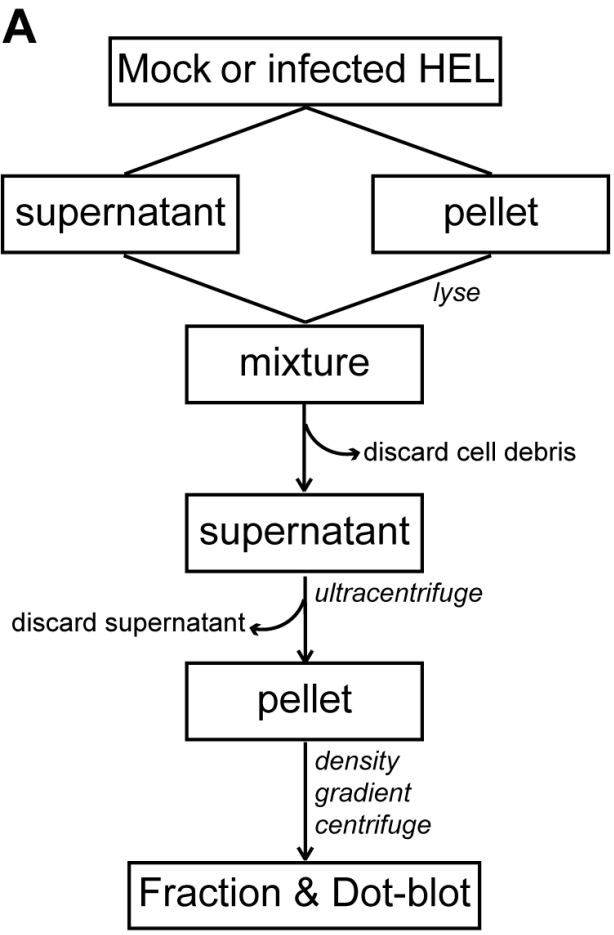
A
Mock or infected HEL
supernatant
pellet
lyse
mixture
discard cell debris
supernatant
ultracentrifuge
discard supernatant
pellet
density gradient centrifuge
Fraction & Dot-blot

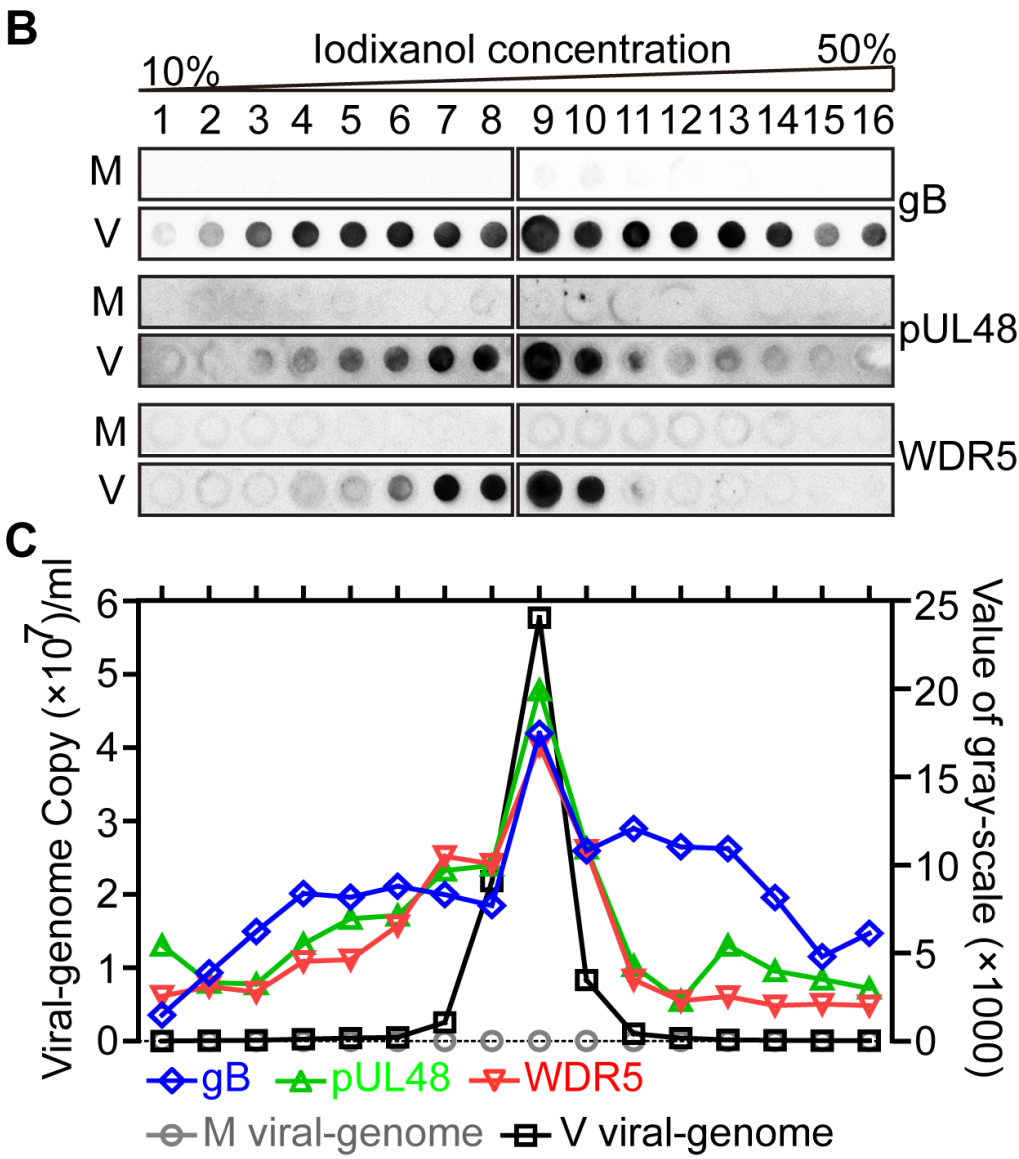
B
Iodixanol concentration
10%
50%
1 2 3 4 5 6 7 8 9 10 11 12 13 14 15 16
M
V
gB
pUL48
WDR5
C
Viral-genome Copy (×10^7)/ml
Value of gray-scale (×1000)
gB
pUL48
WDR5
M viral-genome
V viral-genome

FIG8

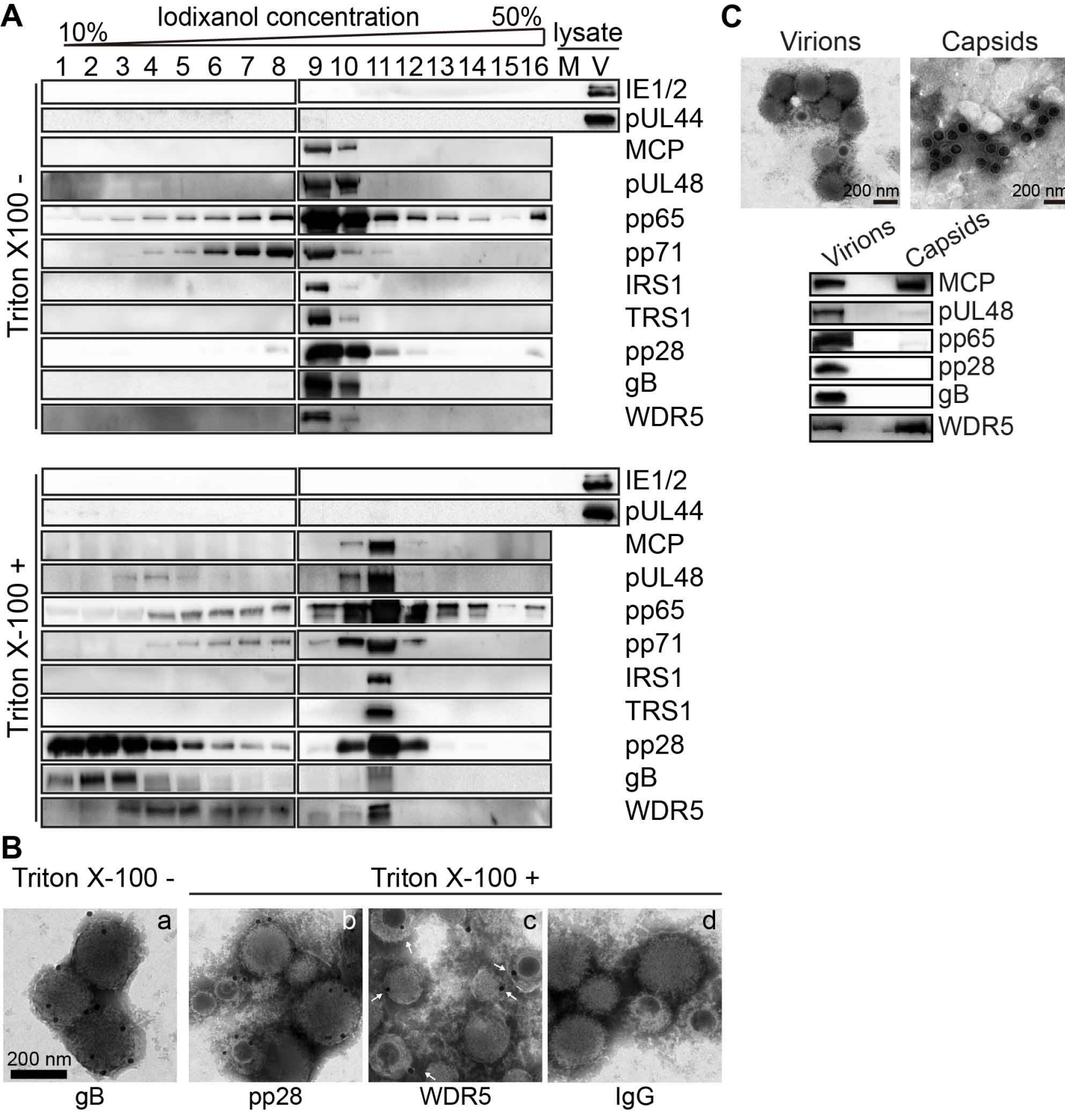
A
Iodixanol concentration
10%
50%
lysate
1 2 3 4 5 6 7 8 9 10 11 12 13 14 15 16 M V
Triton X100 -
Triton X-100 +
IE1/2
pUL44
MCP
pUL48
pp65
pp71
IRS1
TRS1
pp28
gB
WDR5
C
Virions
Capsids
200 nm
MCP
pUL48
pp65
pp28
gB
WDR5
B
Triton X-100 -
Triton X-100 +
a
b
c
d
200 nm
gB
pp28
WDR5
IgG

FIG9

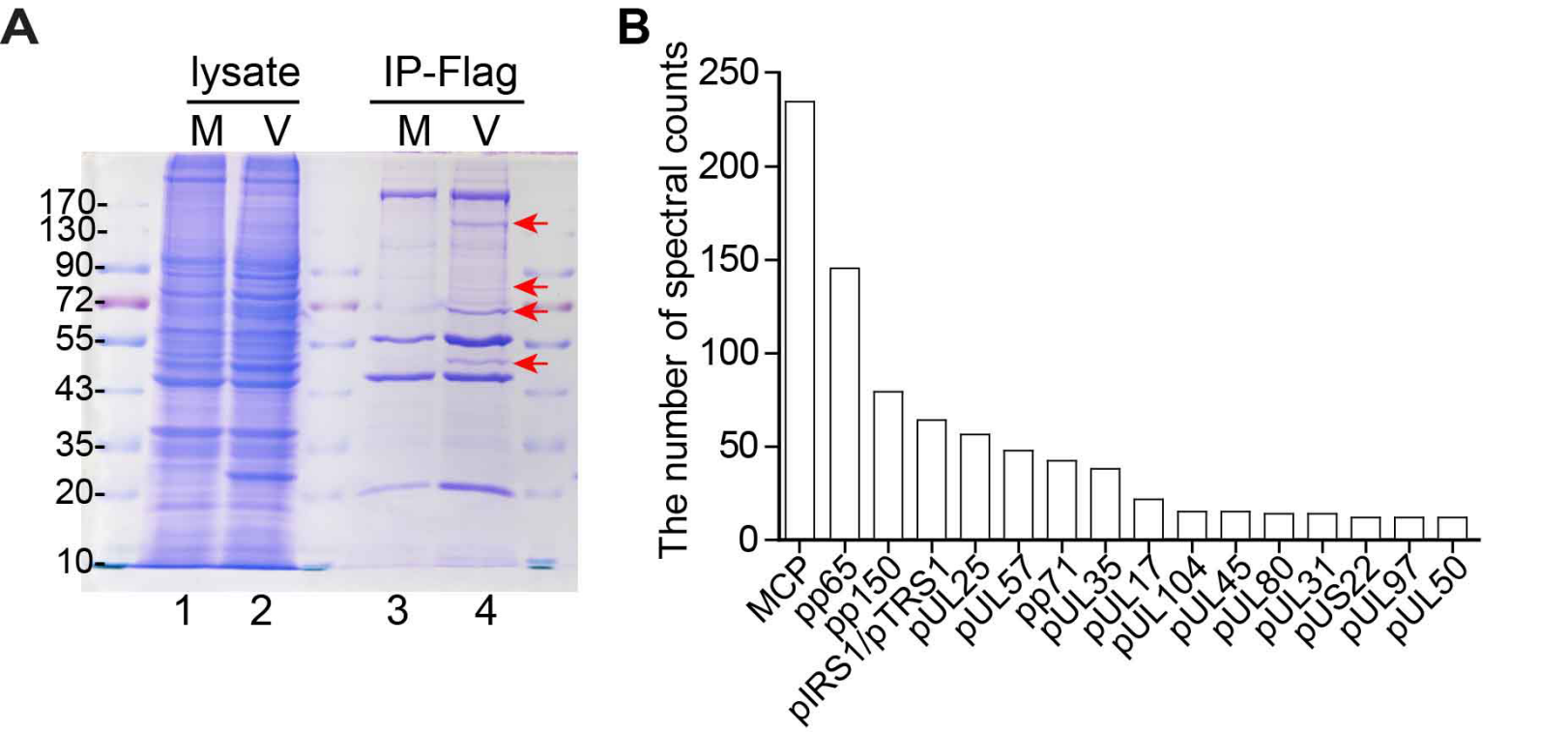
A
lysate
IP-Flag
M V M V
170-
130-
90-
72-
55-
43-
35-
20-
10-
1 2 3 4
B
The number of spectral counts
250
200
150
100
50
0
MCP
pp65
pp150
pIRS1/pTRS1
pUL25
pUL57
pp71
pUL35
pUL17
pUL104
pUL45
pUL80
pUL31
pUS22
pUL97
pUL50

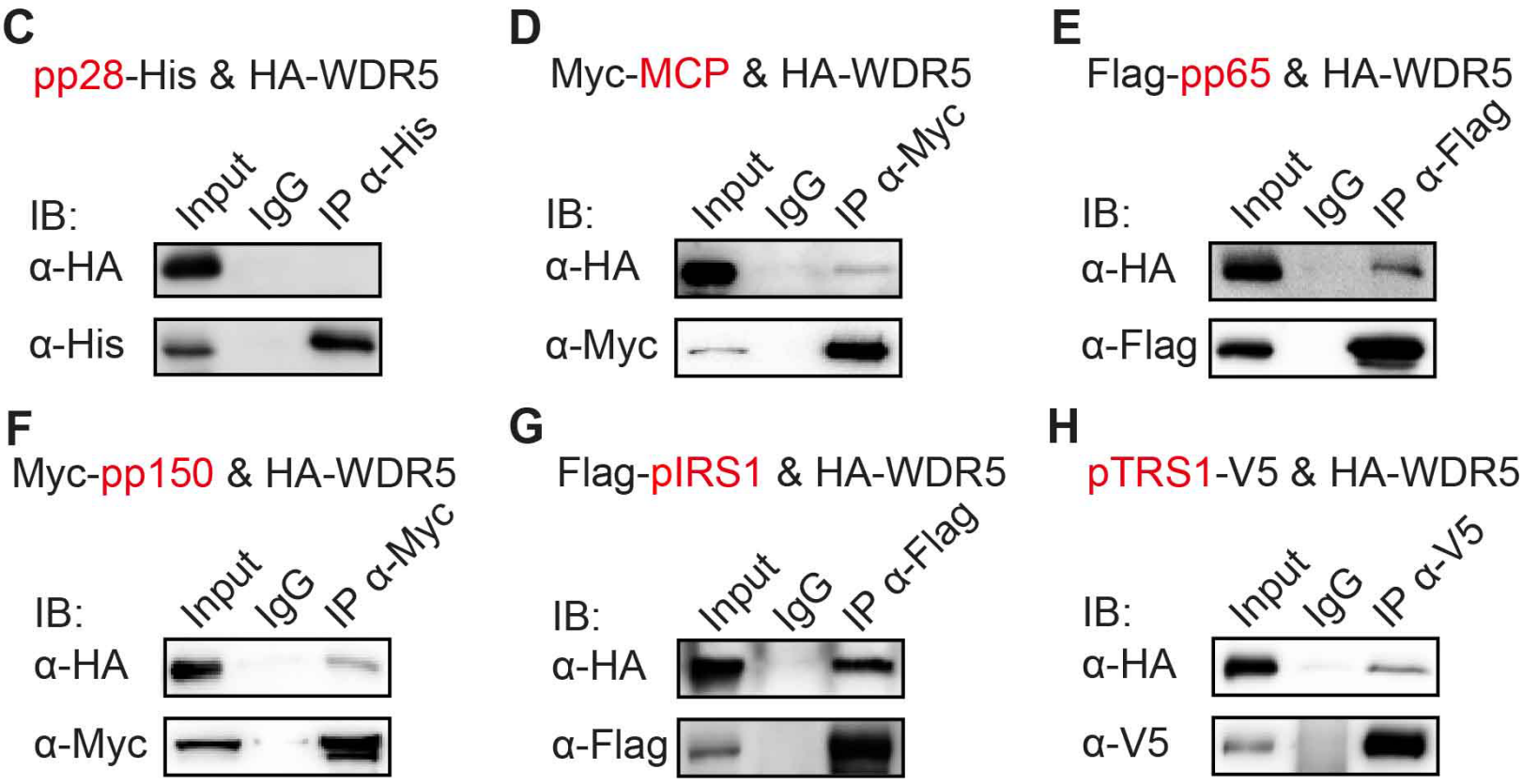
C
pp28-His & HA-WDR5
IB:
Input
IgG
IP α-His
α-HA
α-His
D
Myc-MCP & HA-WDR5
IB:
Input
IgG
IP α-Myc
α-HA
α-Myc
E
Flag-pp65 & HA-WDR5
IB:
Input
IgG
IP α-Flag
α-HA
α-Flag
F
Myc-pp150 & HA-WDR5
IB:
Input
IgG
IP α-Myc
α-HA
α-Myc
G
Flag-pIRS1 & HA-WDR5
IB:
Input
IgG
IP α-Flag
α-HA
α-Flag
H
pTRS1-V5 & HA-WDR5
IB:
Input
IgG
IP α-V5
α-HA
α-V5

FIG10

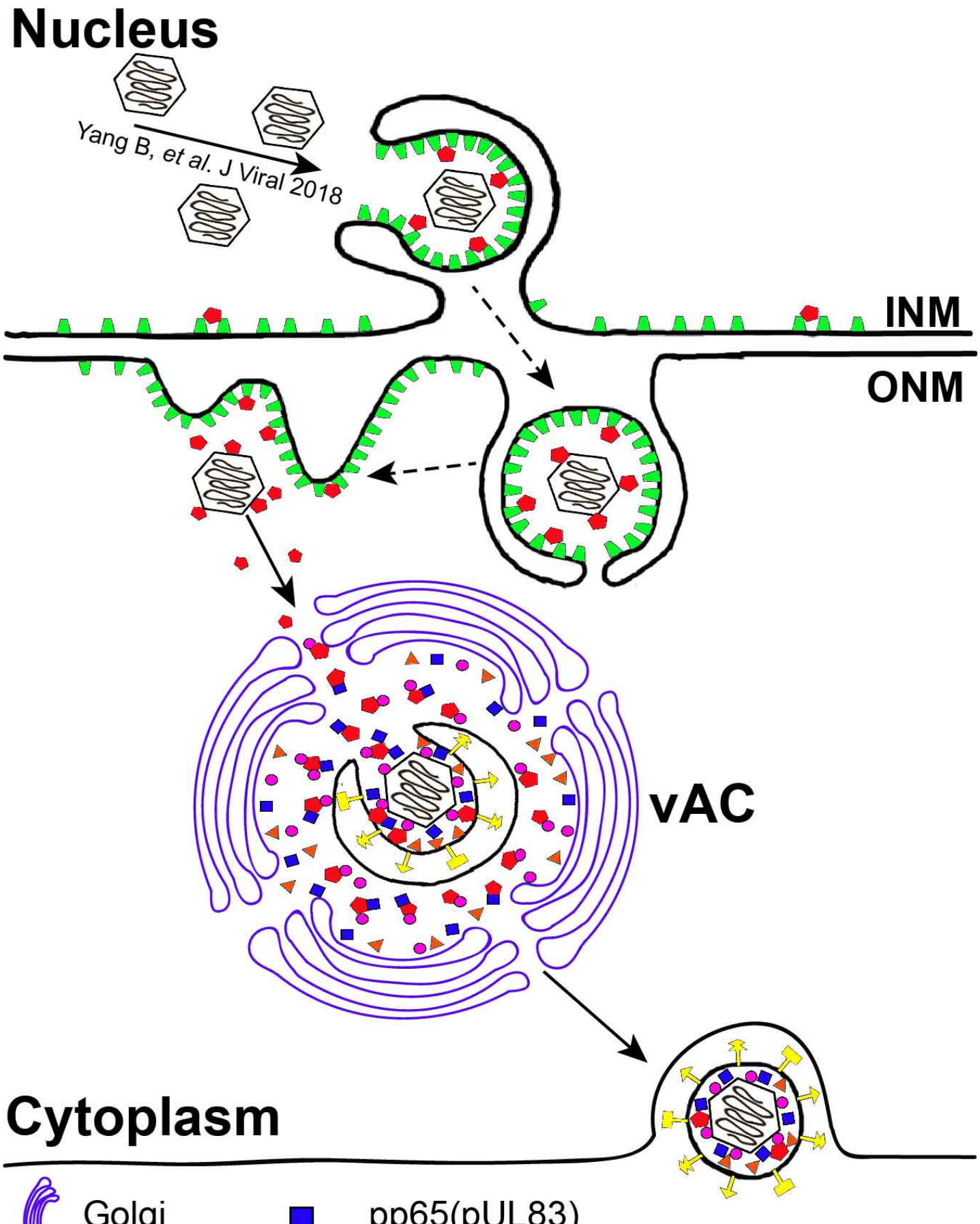
Nucleus
Yang B, et al. J Viral 2018
INM
ONM
vAC
Cytoplasm
Golgi
pp65(pUL83)
NEC
Other tegument proteins
WDR5
Glycoproteins

Table 1. Primers used in this study

Plasmids	Primers
HA-WDR5	**F** 5'-GGAATTCGGATGGCGACGGAGGAGAAGAAGC-3'
	R 5'-CCGCTCGAGTTAGCAGTCACTCTTCCACAGTT-3'
Flag-WDR5	**F** 5'-GCTCTAGAATGGCGACGGAGGAGAAGAAGC-3'
	R 5'-GGAATTCGGCAGTCACTCTTCCACAGTTT-3'
Flag-pp65	**F** 5'-CGGGATCCATGGAGTCGCGCGGTCGCCGTTGTCC-3'
	R 5'-CGGGGTACCTCAACCTCGGTGCTTTTTGGGCG-3'
pp28-6×his	**F** 5'-CGGGATCCATGGGTGCCGAACTCTGCAAACG-3'
	R 5'-GCTCTAGACTAAAGGGCAAGGAGGCGGCGG-3'
Flag-IRS1	**F** 5'-CGGGATCCATGGCCCAGCGCAACGGCATGTC-3'
	R 5'-GGGGTACCTCAATGATGAACGTGGTGAGGGGCG-3'
6Myc-pp150	**F** 5'-GGCGCGGCAGCCGCTTCAAGTTTGCAGTTTATCGGTCTACAGCG-3'
	R 5'-GAGGTTGATTAGGATCTATCGATCTATTCCTCCGTGTTCTTAATCTTC-3'
6Myc-MCP	**F** 5'-GGCGCGGCAGCCGCTTCAGAGAACTGGTCGGCGCTCGAGCTCC-3'
	R 5'-GAGGTTGATTAGGATCTATCGATTCACGAGTTAAATAACATGGATTG-3'

TABLE 2 Primary and Secondary Antibodies Used in IFA and IB.

Primary Antibody	Host / Isotype	Source / Cat.#
Normal Mouse IgG	Mouse polyclonal	Beyotime/A7028
Epitope tag		
Flag	Mouse monoclonal/IgG1	Sigma/F3165
HA	Mouse monoclonal/IgG1	Sigma/H9658
6×His	Mouse monoclonal/IgG1	Proteintech/66005-1-Ig
6×His	Rabbit polyclonal	Abcam/ab9108
V5	Rabbit polyclonal	Proteintech/14440-1-AP
Myc	Mouse monoclonal/IgG1	Proteintech/66003-2-Ig
Cellular		
WDR5 (36 KDa)	Rabbit polyclonal	Sigma/07-706
WDR5 (36 KDa)	Mouse monoclonal/IgG2b	Abcam/ab56919
WDR5 (36 KDa)	Mouse monoclonal/IgG2b	Santa Cruz/sc-100895
GAPDH (36 KDa)	Rabbit polyclonal	Proteintech/10494-1-AP
GFP (30kDa)	Rabbit polyclonal	Proteintech/50430-2-AP
Lamin B1 (66 KDa)	Rabbit polyclonal	Proteintech/12987-1-AP
β-Actin (43 KDa)	Mouse monoclonal/IgG1	Proteintech/60008-1-Ig
α-Tubulin (50 KDa)	Mouse monoclonal/IgG1	Beyotime/AT819
γ-Tubulin (48 KDa)	Mouse monoclonal/IgG1	Gift from Dr. Yan Zhou in Wuhan University, China
EEA1 (180 KDa)	Mouse monoclonal/IgG1	Abcam/ab70521
58K (96 KDa)	Mouse monoclonal/IgG1	Abcam/ab27043
HCMV		
IE1(UL123) (72 KDa)	Mouse monoclonal/IgG2a	(59)
IE1/2 (UL123/122) (72/86 KDa)	Mouse monoclonal/IgG1	Virusys/P1215
pUL44 (ICP36) (46 KDa)	Mouse monoclonal/IgG1	Virusys/P1202-1
gB (UL55) (52 and 105 KDa)	Mouse monoclonal/IgG1	Virusys/P1201
pp71 (UL82) (71 KDa)	Goat polyclonal	Santa Cruz/sc-33323
pp65 (UL83) (65 KDa)	Mouse monoclonal/IgG1	Virusys/P1205
pp28 (UL99) (28 KDa)	Mouse monoclonal/IgG2a	Virusys/CA004-1
pUL48 (253 KDa)	Rabbit polyclonal	Gift from Dr. Wade Gibson in Johns Hopkins University, U.S. (60)
pIRS1(91 KDa)	Mouse monoclonal/IgG1	Gift from Dr. Thomas E. Shenk in Princeton University, U.S. (61)
pTRS1(84 KDa)	Mouse monoclonal/IgG1	Gift from Dr. Thomas E. Shenk in Princeton University, U.S. (61)
MCP (150KDa)	Mouse monoclonal/IgG2a	(62)
MCMV		
mIE1 (m123) (89 KDa)	Mouse Monoclonal/IgG1	Gift from Dr. Qiyi Tang in Howard University College of Medicine, U.S. (63)

Secondary antibody	Host / Isotype	Source / Cat.#
Peroxidase-anti-Mouse IgG	Goat	Jackson ImmunoResearch Laboratories/115-035-003
Peroxidase-anti-Rabbit IgG	Goat	Jackson ImmunoResearch Laboratories/111-035-003
Peroxidase-anti-Goat IgG	Donkey	Jackson ImmunoResearch Laboratories/705-035-147
TRITC-anti-Mouse-IgG2b	Goat	Southern Biotech/1090-03
TRITC-anti-Mouse-IgG2a	Goat	Southern Biotech/1080-03
AF488-anti-Mouse-IgG1	Goat	Thermo Fisher/A-21121
AF488-anti-Mouse-IgG2a	Goat	Thermo Fisher/A-21131
AF647-anti-Mouse-IgG1	Goat	Thermo Fisher/A-21240
AF647-anti-Mouse-IgG2a	Goat	Thermo Fisher/A-21241
10 nm-gold-anti-mouse-IgG	Goat	Boster/GA1004